Journal of Quantitative Spectroscopy & Radiative Transfer 255 (2020) 107238

Contents lists available at ScienceDirect

Journal of Quantitative Spectroscopy & Radiative Transfer

journal homepage: www.elsevier.com/locate/jqsrt

A second-order maximum-entropy inspired interpolative closure for radiative heat transfer in gray participating media

Joachim A.R. Sarr*, Clinton P.T. Groth

University of Toronto Institute for Aerospace Studies, 4925 Dufferin Street, Toronto, Ontario, M3H 5T6, Canada

ARTICLE INFO

Article history:
Received 4 December 2019
Revised 31 July 2020
Accepted 2 August 2020
Available online 4 August 2020

Keywords:
Radiatve heat transfer
Higher-order moment closures
Maximum entropy
Optimization
Numerical modelling
Efficiency
Affine combination

ABSTRACT

A new interpolative-based approximation to the second-order maximum-entropy, M_2, moment closure for predicting radiative heat transfer in gray participating media is proposed and described. In addition to preserving many of the desirable mathematical properties of the original M_2 closure, the proposed interpolative approximation provides significant reductions in computational costs compared to the costs of the original M_2 closure by avoiding repeated numerical solution of the corresponding optimization problem for entropy maximization. Theoretical details of the proposed interpolative-based closure, along with a description of an efficient Godunov-type finite-volume scheme that has been developed for the numerical solution of the resulting system of hyperbolic moment equations, are presented. The finite-volume method makes use of limited linear solution reconstruction, multi-block body-fitted quadrilateral meshes with anisotropic adaptive mesh refinement (AMR), and an efficient Newton-Krylov-Schwarz (NKS) iterative method for solution of the resulting non-linear algebraic equations arising from the spatial discretization procedure. The predictive capabilities of the proposed interpolative M_2 closure are assessed by considering a number of model problems involving radiative heat transfer within one- and two-dimensional enclosures, the results for which are compared to solutions of the first-order maximum entropy, M_1, moment closure, as well as those of the more commonly adopted spherical harmonic moment closure techniques (first-order P_1 and third-order P_3) and the popular discrete ordinates method (DOM). The latter is used as a benchmark for comparisons, whenever exact solutions are not available. The numerical results illustrate the promise of the proposed M_2 closure, with the closure outperforming the M_1, P_1 and P_3 closures for virtually all cases considered.

1. Introduction

Radiative heat transfer is important in a wide variety of scientific and engineering applications, including the thermal sciences and combustion. The transport of radiative energy is governed by the radiative transfer equation (RTE) [1], a complex integro-differential equation of high dimensionality for which there exists no general analytical solution. One must therefore rely on approximate solution techniques and numerical methods in order to obtain predictions of the radiative quantities of interest.

One of the most widely used approximate techniques for solving the RTE is the discrete ordinates method (DOM) [2] which is based on a direct discretization of the angular dependence of the radiative intensity distribution and is generally used in conjunction with space marching techniques. While extremely efficient for problems involving relatively simple geometry and simplified physics (e.g., non-scattering media), the latter can become inefficient for problems with complex three-dimensional geometries and realistic physics [3], as is the case in many practical applications. The potential computational limitations of the DOM has motivated the investigation of alternative approximate radiation solution techniques, such as the method of moments as originally proposed by Grad [4] in the case of gaskinetic theory. As the name suggests, the method of moments solves directly for just a finite set of angular integrals of the intensity distribution, instead of solving directly for the angular distribution, and this can afford a reduction in computational costs compared to those associated with solving directly the high-dimensional RTE. The resulting system of equations for the finite set of moments can not be readily solved however, as there are more unknowns than equations. An additional relation between the highest order moments (unknown) and the known finite set of lower-order moments is required for closure. The resulting closure relation is generally obtained by making an assumption about the approximate form for the underlying radiative intensity distribution in term of the lower-order moments.

* Corresponding author.
E-mail address: joachimandre.sarr@mail.utoronto.ca (J.A.R. Sarr).

https://doi.org/10.1016/j.jqsrt.2020.107238
0022-4073/

The most common approach for providing closure to the system of angular moment equations arising from the RTE is the spherical harmonic P_N approximation [5], where N refers to the order of the approximation. In the P_N moment closures, the radiative intensity distribution is approximated by a series expansion in terms of spherical harmonic functions as well as the know finite set of moments. An analytical expression for the highest-order moments in term of the lower-order moments, or closure relation, can then be obtained, for any order N, by appropriately integrating the approximate form of the distribution with respect to its angular variables. The lowest-order spherical harmonics approximation, namely the first-order P_1 closure has been extensively used to provide approximate solutions to the radiation heat transfer equation [6–9], due to its simplicity and relatively low computational costs. However, because the closing relation for the P_1 approximation is similar to that of an isotropic distribution with the same energy density, the latter closure cannot properly describe highly anisotropic distributions of radiation. Beyond the P_1 closure, even-order P_N approximations are known to be less accurate than their odd-lower-order counterparts [10] and thus odd-order spherical harmonic closures are generally considered. While the P_3 approximation can capture more anisotropy in the distribution than its first-order counterpart, this comes at the expense of substantially increased computational costs. Moreover, the convergence of the P_N closures is rather slow with increasing N [11]. Another important drawback of the P_N closures is that the approximate forms of the distribution of radiative intensity are not strictly positive and the closures are not valid for the full range of physically realizable moments at any order.

More recently, closure techniques based on the principle of maximization of entropy, or maximum entropy, M_N, closures [12], where N again refers to the order of the approximation, have received considerable interest in the field of radiation modelling. The M_N closures take the most likely form of the angular distribution among all the possible ones reproducing a given finite set of moments [13]. In addition to this highly desirable feature for an accurate closure, the M_N hierarchy of models possesses many desirable mathematical and numerical properties, including moment realizability and hyperbolicity. Furthermore, even the lower-order approximations including the first-order M_1 maximum entropy moment closure, can accurately capture a wide range of optical conditions (both equilibrium and non-equilibrium regimes). The M_1 moment closure for gray gas, for which there exists a closed form analytical expression for the closing relation, has been studied by a number of researchers [14,15]. Its predictive capabilities were observed to be superior to those of the P_1 closure for a relatively wide range of optical conditions. However, one important limitation of the M_1 closure is its inability to properly capture situations where there is more than one primary direction for the propagation of the radiative energy. In these cases, the M_1 closure produces a nonphysical discontinuity in the radiative energy density [14]. For this reason, there has been considerable interest in the higher-order members of the maximum entropy moment closure hierarchy, beginning with the second-order M_2 maximum entropy closure. Unfortunately, the application of the higher-order M_N closures is made difficult due to the lack of closed-form analytical expressions for the closing fluxes, even for problems involving gray gases. Repeated numerical solution of the optimization problem for entropy maximization is therefore required, which can make the application of the higher-order M_N closures computationally prohibitive. In spite of these difficulties, in a previous study Hauck [16,17] explored the predictive capabilities of the higher-order maximum entropy moment closures (i.e., M_2, M_3, M_4 and M_5) for various test problems involving gray-gas radiative heat transfer in one-dimensional slab geometries. In this study, the solutions of the aforementioned M_N closures were obtained by solving the optimization problem for entropy maximization via a numerical approach. Furthermore, Hauck compared the predictions of the aforementioned M_N closures to those of the M_1 closure, as well as those obtained using the P_1 and P_3 spherical harmonic approximations and clearly demonstrated that the higher-order M_N closures provided significantly improved predictions of radiative heat transfer, relative to the M_1 closure. Similar results have been obtained by Monreal and Frank [18], who proposed an analytical approximation for the M_2 closing relation in the one-dimensional case.

Motivated by a desire for moment closures for radiative transport applications which have the desirable properties of the high-order M_N closures without the prohibitive computational costs associated with repeated solution of the optimization problem for entropy maximization, Pichard et al. [19] recently proposed an interpolative-based approximation of the closure relation for the M_2 closure in multiple space dimensions. Similar interpolative-based variants of maximum entropy closures have been considered previously by McDonald and Groth [20] and McDonald and Torrilhon [21] in the case of gaskinetic theory. In the approach of Pichard et al. [19], an approximation of the closing flux in one space dimension, obtained by means of a convex combination between the boundaries, with the convex interpolant obtained through fitting of the numerical values obtained from the solution of the optimization problem, was first proposed. An extension to multiple space dimensions was then developed by means of interpolation with respect to both the first- and second-order moments for all of moment space as defined by the conditions for the realizability of the predicted moments. The necessary and sufficient conditions for the latter for moments up to second-order in multiple space dimensions were first formulated by Kershaw [22]. In spite of this step forward, some problematic issues can be identified related to the resulting closure of Pichard et al. In particular, a closer investigation by the present authors has revealed that some of the expressions used in the previous procedure proposed for the evaluation of the interpolant on the boundaries of moment space do not match the corresponding exact analytical expressions on these boundaries. This apparent mismatch in the values produces discontinuous solution behaviour near the boundaries of the realizability domain and, as a consequence, the resulting interpolative-based closure is definitely not globally hyperbolic. The latter poses problems for practical simulations.

In this study, an alternative interpolative-based analytical approximation to the M_2 maximum entropy closure for gray radiative heat transfer in multiple space dimensions is therefore proposed. The objective is to mimic as closely as possible the solution quality and desirable properties of the M_2 closure while avoiding the computationally expensive iterative numerical solution associated with the entropy maximization problem in practical simulations. As they are a key ingredient in the construction of the interpolative closure, the necessary and sufficient conditions for realizability of the predicted moments as defined by Kershaw [22] are first reviewed and a variant of the proof of sufficiency is given. The latter is done by proving the existence of a distribution that reproduces the moments satisfying the necessary conditions and is non-negative everywhere within the realizability domain. The new approximation for the M_2 closure is then obtained by carefully studying the maximum-entropy solution within the realizability domain and then making a careful choice of the interpolant such that it exactly reproduces the known analytical expressions for the closure on the boundaries of the realizability domain and also approximates pre-computed numerical solutions of the entropy optimization problem within the interior of this domain. The exact expressions of the closure relations on the boundaries are obtained by relating them to derived forms for the distribution at the boundaries. It is also shown by numerical experiment that the newly developed interpolative-based closure appears to remain hyperbolic

everywhere within the space of physically realizable moments. Finally, an efficient Godunov-type finite-volume scheme is proposed and developed for the numerical solution of the resulting system of hyperbolic moment equations arising from the M_2 interpolative-based closure. The predictions of the M_2 closure are then assessed through comparisons to additional numerical results obtained for the M_1, P_1 and P_3 moment closures, as well as results obtained using the DOM, for a number of representative problems. The solutions of the DOM are used here as a reference for comparison, whenever exact analytical solutions of the RTE are not available for a given test problem. The radiative heat transfer problems of interest include gray radiative heat transfer between parallel plates as well as within two-dimensional rectangular domains.

2. Radiation transport in gray participating media

The transport of radiant energy in physical space, $\vec{x}$, and time, t, in the direction, $\vec{s}$, at a given wave number, η, in a radiatively participating media with absorption coefficient, $\kappa_\eta = \kappa_\eta(\vec{x}, t)$, and scattering coefficient, $\sigma_{s\eta} = \sigma_{s\eta}(\vec{x}, t)$, is described by the radiative transfer equation [1], which has the form

$$\frac{1}{c}\frac{\partial I_\eta}{\partial t} + \vec{s}.\vec{\nabla} I_\eta = \kappa_\eta I_{b\eta} - (\kappa_\eta + \sigma_{s\eta}) I_\eta + \frac{\sigma_{s\eta}}{4\pi}\int_{4\pi} I_\eta(\vec{s}')\Phi_\eta(\vec{s}', \vec{s})\mathrm{d}\Omega', \tag{1}$$

where c is the speed of light in a vacuum, $I_\eta = I_\eta(\vec{x}, \vec{s}, t)$ is the spectral radiative intensity distribution, $I_{b\eta} = I_{b\eta}(T)$ (where $T = T(\vec{x}, t)$ is the temperature field) is the spectral Planck function or black-body intensity, Ω denotes solid angle, and $\Phi_\eta(\vec{s}', \vec{s})$ is the scattering phase function. The latter describes the probability that a ray travelling in direction, $\vec{s}'$, will be scattered into direction, $\vec{s}$, and is also a function of location in space and time. The subscript, η, indicates a spectrally varying quantity. For gray media, for which the radiative properties are independent of wave number, i.e., $\kappa_\eta = \kappa$ and $\sigma_{s\eta} = \sigma_s$, integrating the RTE, Eq. (1), over the full spectrum and assuming isotropic scattering, i.e., $\Phi(\vec{s}', \vec{s}) = 1$, yields the following form for the RTE [1]

$$\frac{1}{c}\frac{\partial I}{\partial t} + \vec{s}.\vec{\nabla} I = \kappa I_b - (\kappa + \sigma_s) I + \frac{\sigma_s}{4\pi}\int_{4\pi} I(\vec{s}')\mathrm{d}\Omega', \tag{2}$$

where $I = \int_0^\infty I_\eta d\eta$ is the total, spectrally integrated radiative intensity distribution.

The RTE for a gray medium, as represented by Eq. (2), is a complex equation with high dimensionality (6 independent variables) for which there exists no general exact analytical solution. As such, one must therefore rely on numerical techniques based on approximate treatments on the independent variables. The temporal and spatial dependencies can be treated using standard finite-volume techniques for hyperbolic equations. For the treatment of the angular dependence of the radiative intensity distribution, different approximate models can be considered, including the discrete ordinates method, as well as moment closures based on spherical harmonic approximations and the principle of entropy maximization.

2.1. Discrete ordinates method (DOM)

In the DOM, angular quadrature is used to transform the equation of radiative transfer into a set of partial-differential equations (PDEs) with only spatial and temporal dependence. The angular discretization technique makes use of the assumption that the radiation is transported only along a finite set of discrete directions, instead of the effectively infinite number of directions allowed in Eq. (2) by a continuous representation of the solid angle. In other words, the solid angle is divided into a finite number, M, of discrete directions (or ordinates) $\vec{s}_m$. In this way, the RTE is transformed into a system of M coupled equations given by

$$\frac{1}{c}\frac{\partial I_m}{\partial t} + \vec{s}_m \cdot \vec{\nabla} I_m = \kappa I_b - (\kappa + \sigma_s) I_m + \frac{\sigma_s}{4\pi}\sum_{n=1}^{M} w_n I_n, \tag{3}$$

where the subscript m denotes the discrete ordinate direction, I_m is the intensity in the m^{th} direction and w_m is the quadrature weight associated with the direction $\vec{s}_m$. Several quadrature rules have been developed for the DOM, including the S_N schemes of Lathrop and Carlson [23] and the T_N schemes of Thurgood *et al.* [24]. The T_4 quadrature scheme is used in this study for all of the reported DOM simulation results.

The DOM has been used extensively to provide approximate solutions to the RTE due to its good balance between accuracy and computational efficiency. However, this direct discretization technique is associated with two major limitations [25]: false scattering and ray effects. The former is due to the spatial discretization of the RTE whereas the latter is related to the discretization of the angular distribution of the radiative intensity. Several approaches have been proposed in order to cope with such issues [24,26–30]. Additionally, as mentioned in the introduction, the space marching techniques commonly used to solve the resulting discretized equations of the DOM can be extremely efficient for relatively simple geometries and physics; however, the space marching techniques may exhibit poor convergence for applications involving complex three-dimensional geometries and complex physics [3] (e.g., media with high scattering, turbulent reactive flows, etc.).

3. Moment closure methods for solution of the RTE

An alternative approach to the treatment of the angular dependence of the radiative intensity distribution as carried out in the DOM involves instead solving directly for the angular integrals or macroscopic moments of the distribution. These angular moments, $I^{(n)}$, are taken with respect to angular weights $\vec{s}^{\,n} = \vec{s}\otimes \overset{n}{\ldots} \otimes\vec{s}$, $n = 0, \ldots, \infty$, whose entries form a monomial basis, and have the form

$$\begin{aligned} I^{(n)}(\vec{x}, t) &= \langle \vec{s}^{\,n} I(\vec{x}, \vec{s}, t)\rangle = \int_{4\pi} \vec{s}^{\,n} I(\vec{x}, \vec{s}, t)\,\mathrm{d}\Omega \\ &= \int_0^{2\pi}\int_0^{\pi} \vec{s}^{\,n} I(\vec{x}, \vec{s}, t)\sin\theta\,\mathrm{d}\theta\,\mathrm{d}\psi. \end{aligned} \tag{4}$$

Taking angular integrals of the RTE, Eq. (2), results in a system of moment equations of infinite size characterizing uniquely an arbitrary distribution. Solving such an infinite system of equations is however obviously unfeasible from a practical numerical point of view. Instead, a reduced finite set of moments and their transport equations are considered in practice. However, a solution to the so-called closure problem is then required in this case as the resulting system of transport equations for the finite set of moments generally involves the next higher-order moment. In particular, additional expressions relating the next higher-order moment to the known lower-order moments are required for closure. These so-called closing relations are usually obtained by approximating the underlying positive angular distribution in terms of the known finite set of moments. There however exists a wide range of possible forms for such an approximate distribution. In fact, there is effectively an infinite set of possible distributions sharing the same set of known lower-order moments. Moreover, the choice of the approximate form generally dictates many of the important mathematical properties of the resulting closed system of moment equations: namely the realizablility of the predicted moments and hyperbolicity of the moment equations. A set of moments is said to be physically realizable if there exists a strictly positive-valued dis-

tribution of the radiative intensity that will yield the given moments [31]. The set of all realizable moments up to a given order n then defines the so-called n-dimensional phase space of physically realizable moments and is denoted here as $\mathcal{R}^n$. This region is generally described by a set of inequalities on the values of the moments: the so-called realizability conditions. In this study, approximate forms for the angular distribution resulting from the spherical harmonic approximation as well as the principle of maximization of entropy will be considered and their application to radiative transport in gray media will be the primary focus.

An important consideration for the moment closure techniques outlined above is the selection or choice of the number of moments to be included in the closure of interest and which are subsequently used to reconstruct the approximate angular intensity distribution. In general, only the zeroth- and first-order moments, namely the radiative energy density $I^{(0)}$ and the radiative heat flux $I^{(1)}$, respectively, are of primary interest in engineering applications. However, in general the more angular moments that are used in the closure to reconstruct the approximate distribution, the wider the range of optical conditions that may be captured accurately by the closure.

3.1. P_N spherical harmonic moment closures

In the spherical harmonic moment closure approximation, the radiative intensity distribution, $I(\vec{x},\vec{s},t)$, is expressed in terms of a series of spherical harmonic functions as [1,5]

$$I(\vec{x},\vec{s},t)=\sum_{n=0}^{N}\sum_{m=-n}^{n}I_n^m(\vec{x},t)Y_n^m(\vec{s}), \tag{5}$$

where N is the order of the highest moment in the closed system, $I_n^m(\vec{x},t)$ are location-dependent coefficients of the series expansion which can be directly related to the know finite set of moments, and $Y_n^m(\vec{s})$ is the spherical harmonic function of degree n and order m having the form

$$Y_n^m\left(\vec{s}\right)=\begin{cases}\cos(m\psi)P_n^m(\cos\theta), & \text{for } m\geq 0,\\ \sin(|m|\psi)P_n^{|m|}(\cos\theta), & \text{for } m<0,\end{cases} \tag{6}$$

where $P_n^m(\cos\theta)$ is the associated Legendre polynomial.

3.2. First-order P_1 spherical harmonic moment closure

The first-order P_1 spherical harmonic moment closure provides closure to the system of transport equations involving just the zeroth- and first-order moments, $I^{(0)}$ and $I_i^{(1)}$, respectively (i.e., a set of four moments in three space dimensions for the radiation intensity and fluxes in each coordinate direction), by approximating the distribution Eq. (5) with $N=1$ in terms of those lower-order moments. The second-order moment, $I_{ij}^{(2)}$, is a dyadic quantity (i.e., a second-order tensor) and is involved in the transport equation for $I_i^{(1)}$. This quantity can be directly expressed in terms of those lower-order moments via integration thereby providing closure to the system of equations. For a gray medium, the resulting closing expression for $I_{ij}^{(2)}$ takes the form

$$I_{ij}^{(2)}=\frac{\delta_{ij}}{3}I^{(0)}, \tag{7}$$

where δ_{ij} is the Kronecker delta. This is the so-called P_1 approximation which is generally considered to be accurate only for optically thick media as it is associated with a nearly-isotropic distribution of the radiative intensity.

3.3. Third-order P_3 spherical harmonic moment closure

For comparisons to the proposed M_2 interpolative closure, the P_3 moment closure is also considered here. The P_3 approximation involves moments of order up to three (i.e., $I^{(0)}$, $I_i^{(1)}$, $I_{ij}^{(2)}$, and $I_{ijk}^{(3)}$), where the transport equations for the third-order moments involve the fourth-order moments, $I_{ijkl}^{(4)}$, which are generally unknown but can be expressed in terms of the lower order moments by making use of the form for the distribution given in Eq. (5) with known angular moments up to third-order. The fourth-order angular moments, $I_{ijkl}^{(4)}$, of this distribution can be evaluated directly yielding the following closing relations:

$$\begin{aligned} I_{iiii}^{(4)}&=-(3/35)I^{(0)}+(6/7)I_{ii}^{(2)}, & I_{iiij}^{(4)}&=(3/7)I_{ij}^{(2)},\\ I_{iijj}^{(4)}&=(4/35)I^{(0)}-(1/7)I_{kk}^{(2)}, & I_{iijk}^{(4)}&=(1/7)I_{jk}^{(2)}. \end{aligned} \tag{8}$$

It has been shown previously that the third-order P_3 spherical harmonic approximation yields significantly improved predictions compared the P_1 closure [10]. However, this comes at the expense of significantly increased computational costs. Moreover, higher-order approximations ($N\geq 3$), result in further increases in computational effort, whereas the accuracy improvements with increasing N are somewhat more modest [32,33]. For these reasons, it is felt that the P_3 approximation provides a reasonable balance between accuracy and computational costs.

3.4. M_N maximum-entropy moment closures

For a given wave number, η, or frequency, the radiative intensity distribution, I_η, in the maximum-entropy moment closures is approximated by a distribution that maximizes the radiatve entropy, $H_R(I_\eta)$, defined by

$$H_R(I_\eta)=\langle h_R\rangle=\int_{4\pi}h_R(I_\eta)\mathrm{d}\Omega, \tag{9}$$

and has a known finite set of moments $E_\eta^{(n)}$, $n=0,\ldots,N$, where N is the order of the highest moment in the closed system of moment equations. In Eq. (9), h_R is the radiative entropy density, which corresponds to the entropy for Bose-Einstein statistics in this case and is given by

$$h_R(I_\eta)=\frac{2k\eta^2}{c}[(n+1)\ln(n+1)-n\ln(n)],\qquad n=\frac{I_\eta}{2hc\eta^3}, \tag{10}$$

where n is the occupation number, h and k are the Planck and Boltzmann constants, respectively. The problem of finding a distribution, I_η, that maximizes the radiative entropy given by Eqs. (9) and (10) and subject to the constraints that a finite set of its angular moments, $E_\eta^{(n)}$, $n=0,\ldots,N$, are specified and known can be reformulated as an optimization problem of the form

$$\begin{aligned} &\mathcal{I}_\eta=\dashv\nabla\}\,\Updownarrow\dashv\S_{I_\eta}\mathcal{H}_{\mathcal{R}}(\mathcal{I}_\eta)\\ &\text{s.t.}\quad\langle\vec{s}^{\star(n)}I_\eta\rangle=E_\eta^{(n)},\quad n=0,\ldots,N. \end{aligned} \tag{11}$$

The Lagrangian of this optimization problem is

$$\mathcal{L}(I_\eta,\boldsymbol{\alpha})=H_R(I_\eta)-\boldsymbol{\alpha}^T(\langle\underline{\mathrm{m}}(\vec{s})I_\eta\rangle-\mathbf{E}_\eta), \tag{12}$$

where $\boldsymbol{E}_\eta$ is a vector containing all the independent entries of $E_\eta^{(n)}$, $n=0,\ldots,N$, $\boldsymbol{m}(\vec{s})$ is a vector containing all the independent entries of $\vec{s}^{\star(n)}$, $n=0,\ldots,N$, and $\boldsymbol{\alpha}$ is the vector of Lagrange multipliers associated with the moment constraints. The entropy maximizing distribution, which satisfies $\partial\mathcal{L}(I_\eta,\alpha)/\partial I_\eta=0$, then takes the form [12]

$$\mathcal{I}_\eta(\boldsymbol{\alpha},\boldsymbol{m})=2\,hc\eta^3\left[\exp\left(\frac{c^2h\eta}{k}\boldsymbol{\alpha}^T\boldsymbol{m}(\vec{s})\right)-1\right]^{-1}. \tag{13}$$

In the case of radiation transport in gray media, the distribution function Eq. (13) can be integrated over the full spectrum of frequencies ($\eta\in[0,\infty]$), yielding

$$\mathcal{I}(\boldsymbol{\alpha},\boldsymbol{m})=\frac{\sigma_{stef}}{\pi}\left[\boldsymbol{\alpha}^T\boldsymbol{m}(\vec{s})\right]^{-4}, \tag{14}$$

where $\sigma_{stef} = 2\pi^5 k^4/15c^2h^3$ is the Stephan Boltzmann constant.

In Eq. (14), the radiative intensity distribution is not given explicitly but is rather expressed in terms of the Lagrange multipliers, $\boldsymbol{\alpha}$, which have to be determined from the set of nonlinear coupled algebraic equations $\langle \boldsymbol{m}(\vec{s})\mathcal{I}\rangle = \boldsymbol{E}$. With the exception of the gray M_1 model [12], there exists no analytical expressions for the Lagrange multipliers in terms of the angular moments and, as such, the Lagrange multipliers must therefore be determined numerically by solving the Lagrangian dual optimization problem for entropy maximization given by

$$arg\, max_{\boldsymbol{\alpha}}\{\mathcal{L}^*(\boldsymbol{\alpha})\}, \tag{15}$$

where $\mathcal{L}^*(\boldsymbol{\alpha})$ is the Legendre transform of $\mathcal{L}(I, \boldsymbol{\alpha})$, and has the form

$$\mathcal{L}^*(\boldsymbol{\alpha}) = -\frac{\sigma_{stef}}{3\pi}\left\langle \left[\boldsymbol{\alpha}^T \boldsymbol{m}(\vec{s})\right]^{-3}\right\rangle - \boldsymbol{\alpha}^T \boldsymbol{E}. \tag{16}$$

Once the Lagrange multipliers have been determined, the closing flux for the closure can be evaluated using numerical quadrature. However, it should be noted that the repeated solution of the optimization problem defined by Eq. (15) whenever an update of the radiation solutions is required can become very expensive computationally, particularly as the number of moments increases as is the case for the higher-order maximum entropy closures in multiple space dimensions. For this reason, interpolative-based approximations are proposed in what follows for the closing fluxes of the gray M_2 closure, which are based on pre-computed solutions of the optimization problem associated with entropy maximization for sets of angular moments up to second-order spanning the associated realizable space.

3.5. First-order M_1 maximum-entropy moment closure

The first member of the maximum-entropy hierarchy for gray media is the first-order M_1 closure. Unlike other high-order members of this hierarchy, analytical expressions for the Lagrange multipliers in terms of the known set of moments exist in the case of a gray medium for the M_1 closure. Similar, to the P_1 spherical harmonic approximation, the M_1 model achieves closure by using the entropy maximizing distribution of Eq. (14) and expressing the second-order moment dyad in terms of the lower-order moments, i.e., $I^{(2)} = I^{(2)}(I^{(0)}, I^{(1)})$. Another feature of the first-order closure is that the anisotropy in the underlying radiative distribution lies in the direction of the first-order moment vector or flux, $I^{(1)}$. This in turn implies that the radiative intensity distribution is symmetric with respect to the direction of $N^{(1)} = I^{(1)}/I^{(0)}$. Using this property, Levermore [34] previously derived an expression for the closing flux of the M_1 closure which takes the form

$$I^{(2)} = N^{(2)} I^{(0)}, \qquad N^{(2)} = \frac{1-\chi}{2}\vec{\vec{I}} + \frac{3\chi - 1}{2}\vec{n}\otimes\vec{n}, \tag{17}$$

where χ is the well-known Eddington factor and, for the gray M_1 closure, is given by

$$\chi = \frac{3 + 4\|N^{(1)}\|^2}{5 + 2\xi} \quad , \quad \xi = \sqrt{4 - 3\|N^{(1)}\|^2}, \tag{18}$$

and where $N^{(n)} = I^{(n)}/I^{(0)}$ are the n^{th}-order normalized moments, $\vec{\vec{I}}$ is the identity dyad, and $\vec{n} = N^{(1)}/\|N^{(1)}\|$ is the unit vector in the direction of the first-order moment.

In spite of its ability to capture a wider range of optical conditions than the P_1 model, the M_1 closure is known to produce nonphysical discontinuities in the radiative energy density and also generally provide inaccurate predictions of radiative quantities for situations in which beams of photons travelling in opposite directions cross [14]. In fact, when the zeroth- and first-order angular moments are the only available information for reconstructing a given distribution, the only possible form for the latter in the case of crossing beams with zero net flux is that of an isotropic distribution, even though the underlying angular distributions are highly non-isotropic. This issue can however be remedied by considering high-order members of the maximum-entropy hierarchy.

3.6. Second-order M_2 maximum-entropy moment closure

The next member of the maximum-entropy hierarchy for gray media is the second-order M_2 closure and is the primary focus of the present study. In a procedure similar to that described for the M_1 closure, transport equations for known moments up to second-order are closed by assuming an entropy maximizing distribution and subsequently expressing the third-order closing moments (second-order moment fluxes), $I^{(3)}$, in terms of the known moments, i.e., $I^{(3)} = I^{(3)}(I^{(0)}, I^{(1)}, I^{(2)})$ or, in the case of gray media, $N^{(3)} = N^{(3)}(N^{(1)}, N^{(2)})$. Unfortunately, unlike the M_1 closure for a gray medium, it is not possible to obtain a closed-form analytical expression for the closing moment flux of the M_2 closure (in fact, a closed-form analytical expression for the closing flux is only possible for the M_1 model in the case of gray media) and therefore, in the simulations of radiative transport, repeated numerical solution of the optimization problem defined by Eq. (15) would be necessary, making the application of the closure computationally expensive.

To circumvent the need for the costly solutions of the optimization problem to determine the Lagrange multipliers defining the maximum entropy distribution, an alternative interpolative-based approach for accurately approximating the closing flux for the gray M_2 closure is proposed herein which attempts to retain many of the desirable properties of the original model (e.g., moment realizability and hyperbolicity of the moment equations) while resulting in substantially reduced computational costs compared to the repeated solution of the optimization problem. The proposed interpolant is formulated to closely match the form of the M_2 maximum entropy solution within the entire space of physically realizable moments defined by the angular moments up to second-order (i.e., the space defined by the set of necessary and sufficient conditions such that there exists a non-negative distribution reproducing moments of the M_2 closure). More specifically, an affine combination of the known analytical forms of $N^{(3)}$ on the boundaries of realizable space in terms of $N^{(1)}$ and $N^{(2)}$ is adopted as an approximation to the closing relation. The interpolant is then extended to the interior of realizable space via a fitting procedure such that it approximates pre-computed values of $N^{(3)}$ obtained by solving the optimization problem for entropy maximization for moment sets spanning the full range of realizable space. The development and description of the proposed interpolative-based second-order M_2 closure are given below in the section to follow.

It should be noted that several authors have recently developed analytical approximations to the M_2 maximum-entropy moment closure in multi-dimensional space. Firstly, as noted in the introduction, Pichard *et al.* [19] proposed an extension of the previously-developed approximation to the M_2 closure by Monreal and Frank [18] for one space dimension to multiple dimensions. The multi-dimensional interpolative-based M_2 closure proposed by Pichard et al. [19] was formulated for radiative transport obeying Boltzmann statistics. More specifically, their interpolation attempts to mimic the maximum entropy solutions only in the case where the first-order moment, $N^{(1)}$, coincides with one of the eigenvectors of the covariance matrix, $(N^{(2)} - N^{(1)}(N^{(1)})^T)$. Their approximation of the maximum entropy solutions was comprised of several steps. Firstly, an interpolative-based approximation of the closure relation for the M_2 closure, in the case where the covariance matrix has at least two identical eigenvalues, was developed. This approximation was obtained by means of convex combinations between the upper and lower boundaries of the

realizablity constraints on the highest-order moments, the analytical expressions of which are available in this particular case. The approximation was then extended to more general sets of eigenvalues for the covariance matrix, by means of polynomial interpolation, which reproduces known analytical expressions for the closure relations in the case of degenerate eigenvalues, and also reproduces the approximation corresponding to the case with at least two identical eigenvalues. The choice of polynomial interpolation, instead of convex combinations, at this stage of the approximation was justified by the fact that, unlike the case with at least two identical eigenvalues, there exist to date no necessary and sufficient realizability conditions for the third-order moment, $N^{(3)}$, in more general cases. Extension to the full realizability domain for moments up to order two was then achieved by means of convex combinations within the unit ball described by the realizability constraints on the first-order moment. By its construction, the resulting interpolative-based M_2 closure, was proven to be realizable for sets of moments up to second-order for which the covariance matrix has at least two identical eigenvalues and one of its eigenvector is co-linear to $N^{(1)}$. Moreover, the maximum-entropy solutions are only well approximated in a portion of the full realizable space for moments up to second-order. Finally, it can be shown that the description of the closure relations used by Pichard et al. [19] on some of the boundaries of the realizable domain for moments up to second-order is problematic, making the application to the full range of practical simulations very difficult.

More recently, an extended quadrature method of moments (EQMOM)-based second-order moment closure was developed by Li et al. [35], as an approximation to the M_2 maximum-entropy closure. In their approach, the base function used in the EQMOM scheme are β probability density functions. One of the main advantages of this so-called B_2 model of Li et al. [35], compared to the M_2 closure, is the existence of closed-form analytical expressions for the closure relation. Moreover, the B_2 model provides a smooth interpolation between the isotropic and the free-streaming limits. However, the EQMOM-based closure does not really attempt to mimic closely the properties of the M_2 maximum entropy closure and the B_2 model in multiple space dimensions is neither globally realizable nor globally hyperbolic. In fact, Li et al. [35] have shown that the quadrature-based approximation to the M_2 closure is only realizable and hyperbolic in a portion of the realizable space defined by moments up to second-order.

4. Interpolative-based second-order M_2 maximum-entropy moment closure

In this section, the new interpolative-based approximation of the second-order maximum entropy, M_2, closure is formulated for radiative transfer in multi-dimensional, gray, participating media. Our proposed interpolant is formulated such that the known analytical expressions of the closing fluxes on the boundaries of realizable space are exactly reproduced. Using a polynomial interpolation procedure, the affine interpolant is then extended to match identically a range of pre-computed solutions of the optimization problem for entropy maximization for sets of moments spanning the full realizable space for moments up to second-order, as well as derivatives of the highest-order moment on the boundaries. This fitting of the pre-computed solutions is achieved by the use of orthogonal or near orthogonal polynomial basis functions so as to optimize the condition number of the resulting Vandermonde matrix and consequently facilitate the inversion of the latter. The nodes for the interpolation procedure are chosen to coincide with roots of Chebyshev polynomials, which are known to provide quasi-optimal approximation to any given function. In the near vicinity of the boundaries of the realizable moment space, the numerical solution of the highly nonlinear optimization problem for entropy maximization becomes increasingly difficult, due to ill-conditioning of the Hessian matrix. In order to facilitate the solution of the optimization problem in these regions, preconditioning of the Hessian matrix is applied as described in Section 4.3 to follow, which substantially improves the condition number of the Hessian such that its inverse can be computed with good accuracy.

4.1. Necessary and sufficient conditions for realizability of moments up to second-order

As a first step, the necessary and sufficient conditions for realizability of moments up to second-order are presented and given. A proof of sufficiency is also provided. These conditions and the proof were previously established for both one- and multi-dimensional radiative heat transfer problems by Kershaw [22]. They were also key elements in the construction of the previous second-order closures of Pichard et al. [19] and Li et al. [35]; however, as they are crucial to the development of the proposed interpolative-based approximation of the M_2 closure, they are re-summarized here. Note that proof of sufficiency given here is a slight variant of Kershaw's proof and follows that of Monreal and Frank [18,36] for the one-dimensional case, with an extension to the multi-dimensional case.

Realizability of the predicted angular moments of a given closure deals with the issue of whether or not a physically realistic (i.e., strictly positive valued or non-negative) angular distribution of the radiation intensity can be associated with the given set of moments. If such an angular distribution can be identified, then the moment set is deemed to be realizable. The conditions for moment realizability give rise to a set of constraints or realizability conditions on the predicted moments which can be used to define the extent of possible closure solutions in moment space. The approach essentially consists of multiplying a presumed non-negative distribution by a non-negative polynomial test function defined in terms of the angular variables, from which necessary conditions for realizability of the moments can be derived. For a given set of N angular weights, $\mathbf{S}^{(N)} = [1, \vec{s}^{(1)}, \vec{s}^{(n)}, \ldots]^{\mathrm{T}}$, and corresponding moments, $\mathbf{I}^{(N)} = \langle \mathbf{S}^{(N)} I \rangle$, one can construct a polynomial, $\mathcal{P}^{(N)}(\vec{v}) = \mathbf{a}^{\mathrm{T}} \mathbf{S}^{(N)}$, where $\mathbf{a}^{\mathrm{T}}$ are the coefficients of the polynomial. It then follows that for any globally positive-valued angular distribution, I, and polynomial, $\mathcal{P}^{(N)}$, one must have

$$\left\langle ||\mathcal{P}^{(N)}(\vec{v})||^2 I \right\rangle = \mathbf{a}^{\mathrm{T}} \left\langle \mathbf{S}^{(N)} \left[\mathbf{S}^{(N)}\right]^{\mathrm{T}} I \right\rangle \mathbf{a} \geq 0, \tag{19}$$

which, for an arbitrary polynomial, requires that the real symmetric matrix, $\mathbf{M}^{(N)}$, given by

$$\mathbf{M}^{(N)} = \left\langle \mathbf{S}^{(N)} \left[\mathbf{S}^{(N)}\right]^{\mathrm{T}} I \right\rangle, \tag{20}$$

must be positive definite. For situations in which this matrix is negative definite, it follows that the moment set is not consistent with any possible positive-valued distribution, I, and, hence, the moments are not physically realizable. For the M_2 closure and moments up to second-order for an every-where non-negative angular distribution of the radiative intensity, the corresponding necessary conditions on moment realizability, which define the realizability domain for moments up to second order denoted by $\mathcal{R}^2$, can be defined as follows [18,22,36]:

$$\begin{aligned} \mathcal{R}^2 = \{ (I^{(0)}, I^{(1)}, I^{(2)}) \in \mathbb{R}^3 \times \mathbb{R}^{3\times 3}, \quad \text{s.t.} \quad & I^{(0)} \geq 0, \quad \|N^{(1)}\| \leq 1, \\ & N^{(2)} - N^{(1)}(N^{(1)})^T \geq 0, \quad \vec{n}^T N^{(2)} \vec{n} \leq 1 \quad \forall \quad \|\vec{n}\| \leq 1, \\ & tr(N^{(2)}) = 1 \quad \text{and} \quad N^{(2)}_{ij} = N^{(2)}_{ji} \}. \end{aligned} \tag{21}$$

The proof of the existence of a non-negative distribution reproducing moments in $\mathcal{R}^2$ also provides a proof that conditions $\mathcal{R}^2$ are both necessary and sufficient. The former can be demonstrated via the application of a suitable transformation of $\mathcal{R}^2$ such that the

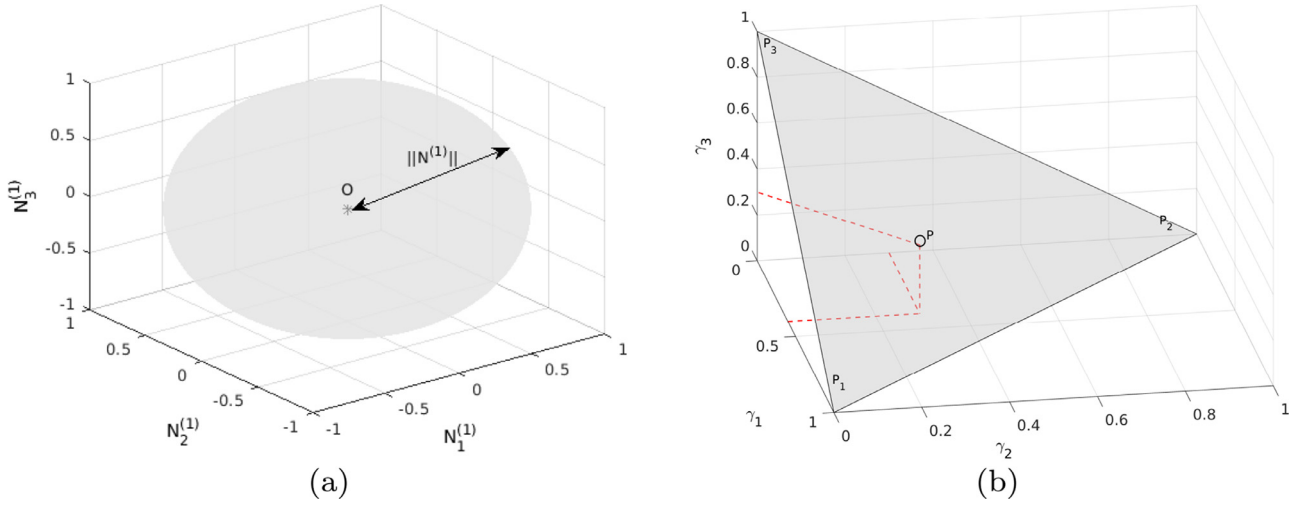

Fig. 1. Realizability Domain, $\mathcal{R}_T^2$, for the M_2 Closure in the frame where $N^{(2)} - N^{(1)}(N^{(1)})^T$ is diagonal positive definite for (a) a fixed set of parameters $\{\gamma_1, \gamma_2, \gamma_3\}$; and (b) a fixed set of moments $\{N'^{(1)}_1, N'^{(1)}_2, N'^{(1)}_3\}$.

form of the distribution can be represented by a convex combination of the distributions on the boundaries of the transformed realizability domain.

The system of equations for moments up to second-order has 10 dependent variables since the zeroth-order moment, $I^{(0)}$, is a scalar, the first-order moment, $I^{(1)}$, is a 3-component vector, and the second-order moment, $I^{(2)}$, is a symmetric second-order dyad or tensor with 6 unique entries. This relatively large set of variables can be reduced to a smaller but essentially equivalent one by an appropriate rotational transformation, Rot, of the coordinate frame such that $\mathrm{Rot}(N^{(2)} - N^{(1)}(N^{(1)})^T)$ is diagonal. In such a rotated frame, the transformed second-order moment, denoted by $N'^{(2)} = \mathrm{Rot}(N^{(2)})$, can be expressed as

$$N'^{(2)} = N'^{(1)}(N'^{(1)})^T + (1 - \|N'^{(1)}\|^2)\mathrm{diag}(\gamma_1, \gamma_2, \gamma_3). \tag{22}$$

where γ_i, $i = 1\ldots3$, are parameters which satisfy the constrains $\gamma_i \geq 0$ and $\sum_{i=1}^{3}\gamma_i = 1$ (please refer to Appendix A). The transformed realizability domain, denoted by $\mathcal{R}_T^2 = \mathrm{Rot}(\mathcal{R}^2)$, then has the following form

$$\mathcal{R}_T^2 = \{(I'^{(0)}, I'^{(1)}, I'^{(2)}) \in \mathbb{R}\times\mathbb{R}^3\times\mathbb{R}^{3\times3},\} \quad \text{s.t.} \quad I'^{(0)} \geq 0, \quad \|N'^{(1)}\| \leq 1,$$
$$0 \leq \gamma_i \leq 1, \quad i = 1\ldots3, \quad \text{and} \quad \sum_{i=1}^{3}\gamma_i = 1\}. \tag{23}$$

The transformed realizability domain, $\mathcal{R}_T^2$, is illustrated in Fig. 1(a), for fixed values of γ_i, $i = 1\ldots3$, and in Fig. 1(b), for a given flux vector $N'^{(1)} = [N'^{(1)}_1, N'^{(1)}_2, N'^{(1)}_3]$. For any realizable first-order moment, $N'^{(1)}$, the second-order moment, $N'^{(2)}$, is realizable if and only if γ_i, $i = 1\ldots3$, satisfy the conditions given in Eq. (23), which describe an equilateral triangle in the coordinates frame $\gamma_1\gamma_2\gamma_3$ as illustrated in Fig. 1(b). As such, any convex combination of realizable moments at the vertices of such a triangle will also be realizable. Inspired by this knowledge, the distribution at any point, P, lying inside the triangle defined by points, P_i, $i = 1\ldots3$, can be expressed as the barycentric interpolant of the values of the distribution evaluated at P_i, I_{P_i}, and written as

$$I_P = \sum_{i=1}^{3}\gamma_i I_{P_i}, \tag{24}$$

where I_{P_i} represent the values of the distribution at P_i, $i = 1\ldots3$, which, as shown in Appendix B, are uniquely determined by a combination of Dirac deltas and take the form

$$I_{P_i} = I'^{(0)}\left[\rho_i^+\delta(\Omega_i - x_i^+) + \rho_i^-\delta(\Omega_i - x_i^-)\right]\delta(\Omega_j - N'^{(1)}_j)\delta(\Omega_k - N'^{(1)}_k), \tag{25}$$

where $(i, j, k) \in (1,2,3)$ with $i \neq j \neq k$ and

$$x_i^{\pm} = \pm\sqrt{1 - \|N'^{(1)}\|^2 + (N'^{(1)}_i)^2}, \tag{26}$$

and

$$\rho_i^{\pm} = \frac{N'^{(1)}_i - x_i^{\mp}}{2x_i^{\pm}}. \tag{27}$$

It is clear that the value of the distribution, I_P, for point, P, given by Eq. (24) is non-negative since it corresponds to a convex combination of non-negative distributions, I_{P_i}, $i = 1\ldots3$. In order to complete the proof of sufficiency, it must be shown that the distribution given by Eq. (24) also reproduces moments lying inside the realizability domain, $\mathcal{R}_T^2$ (see Appendix C). The distributions I_{P_i}, $i = 1\ldots3$, reproduce moments at the vertices of the triangle (P_1, P_2, and P_3), and, as such, any convex combination of these three distributions will therefore reproduce moments lying within the triangle and consequently within $\mathcal{R}_T^2$. This completes the proof.

It is worth pointing out that the distribution of Eq. (24) is similar to that of Kershaw [22] and reduces to his result in the one-dimensional case, i.e., for $N'^{(1)}_2 = 0$ and $N'^{(1)}_3 = 0$. More specifically, in the case where $N'^{(2)}_{11} = 1$, i.e., $\gamma_1 = 1$, Eq. (24) reduces to

$$I_P = I'^{(0)}\left[\frac{1 + N'^{(1)}_1}{2}\delta(\Omega_1 - 1) + \frac{1 - N'^{(1)}_1}{2}\delta(\Omega_1 + 1)\right]\delta(\Omega_2)\delta(\Omega_3), \tag{28}$$

and for $N'^{(2)}_{11} = (N'^{(1)}_1)^2$, i.e., $\gamma_1 = 0$, one obtains

$$I_P = I'^{(0)}\left[\rho_i^+\delta(\Omega_i - x_i) + \rho_i^-\delta(\Omega_i + x_i)\right]\delta(\Omega_j - N'^{(1)}_j)\delta(\Omega_k - N'^{(1)}_k). \tag{29}$$

4.2. Interpolative-based closing relations for M_2 moment closure

With the necessary and sufficient conditions for moment realizability for moments up to second-order established, we can now proceed with the development of a realizable interpolative-based approximation of the M_2 closure for radiative heat transfer in gray participating media. The analytical expressions for the distribution at the vertices of the triangle defined by points (P_1, P_2, P_3) given in Eq. (25) can be used to derive analytical expressions for the closing flux, $N'^{(3)}$, at those points as shown in Appendix B. Similar to the approach used to prove sufficiency of the realizability

Table 1
Exact Analytic Expression of M_2 Closure Relation at the Vertices of the Triangle P_1, P_2, P_3.

Vertex	$N'^{(3)}_{111}$	$N'^{(3)}_{122}$	$N'^{(3)}_{123}$
P_1	$N'^{(1)}_1\left[(N'^{(1)}_1)^2 + (1 - \|N'^{(1)}\|^2)\right]$	$N'^{(1)}_1 (N'^{(1)}_2)^2$	$N'^{(1)}_1 N'^{(1)}_2 N'^{(1)}_3$
P_2	$(N'^{(1)}_1)^3$	$N'^{(1)}_1\left[(N'^{(1)}_2)^2 + (1 - \|N'^{(1)}\|^2)\right]$	$N'^{(1)}_1 N'^{(1)}_2 N'^{(1)}_3$
P_3	$(N'^{(1)}_1)^3$	$N'^{(1)}_1 (N'^{(1)}_2)^2$	$N'^{(1)}_1 N'^{(1)}_2 N'^{(1)}_3$

conditions for moments up to order two, the closing flux relations for the M_2 closure within $\mathcal{R}^2_T$ are approximated by affine combinations of the exact analytical expressions at points P_i, $i = 1 \dots 3$ (see Table 1). The interpolant is chosen such that the closures approximate their corresponding numerical values obtained by solving the optimization problem for entropy maximization, Eq (15), for sets of moments spanning $\mathcal{R}^2_T$. More specifically, the approximation of the closing flux in the rotated frame, $N'^{(3)}$, is assumed to take the form

$$N'^{(3)}_{ijk} = \sum_{i=1}^{3} f(\gamma_i) N'^{(3)}_{ijk}(P_i). \tag{30}$$

where $f(\gamma_i)$ are weighting functions satisfying $\sum_{i=1}^{3} f(\gamma_i) = 1$. Once approximations of the closing moment fluxes in $\mathcal{R}^2_T$ are obtained, the closing relations for $\mathcal{R}^2$ can then be derived through the inverse transformation of $\mathcal{R}^2_T \rightarrow \mathcal{R}^2$ as defined by

$$\begin{aligned} &\mathbb{T} : \mathcal{R}^2_T \rightarrow \mathcal{R}^2(I'^{(0)}, I'^{(1)}, I'^{(2)}) \rightarrow (I^{(0)}, I^{(1)}, I^{(2)}) \\ &\quad \text{s.t.} \quad I'^{(0)} = I^{(0)}, \quad I'^{(1)}_i = R_{ij} I^{(1)}_j, \quad I'^{(2)}_{ij} = R_{im} I^{(2)}_{mn} R_{nj} \end{aligned} \tag{31}$$

where R_{ij} is the rotation matrix such that $R^T(N^{(2)} - N^{(1)}(N^{(1)})^T)R$ is diagonal positive definite.

The third-order normalized moment tensor, $N'^{(3)}$, is symmetric and therefore has just 10 unique entries. Knowledge of just 3 of these entries, namely $N'^{(3)}_{111}$, $N'^{(3)}_{122}$ and $N'^{(3)}_{123}$, is sufficient to obtain values for the remaining 7 entries which can be related to these 3 entries as follows:

$$\begin{aligned}
N'^{(3)}_{222}(N'^{(1)}_1, N'^{(1)}_2, N'^{(1)}_3, \gamma_1, \gamma_2) &= N'^{(3)}_{111}(N'^{(1)}_2, -N'^{(1)}_1, N'^{(1)}_3, \gamma_2, \gamma_1), \\
N'^{(3)}_{333}(N'^{(1)}_1, N'^{(1)}_2, N'^{(1)}_3, \gamma_1, \gamma_2) &= N'^{(3)}_{111}(N'^{(1)}_3, N'^{(1)}_2, -N'^{(1)}_1, 1-\gamma_1-\gamma_2, \gamma_2), \\
N'^{(3)}_{112}(N'^{(1)}_1, N'^{(1)}_2, N'^{(1)}_3, \gamma_1, \gamma_2) &= N'^{(3)}_{122}(N'^{(1)}_2, -N'^{(1)}_1, N'^{(1)}_3, \gamma_2, \gamma_1), \\
N'^{(3)}_{113}(N'^{(1)}_1, N'^{(1)}_2, N'^{(1)}_3, \gamma_1, \gamma_2) &= N'^{(3)}_{122}(N'^{(1)}_3, N'^{(1)}_1, N'^{(1)}_2, 1-\gamma_1-\gamma_2, \gamma_1), \\
N'^{(3)}_{133}(N'^{(1)}_1, N'^{(1)}_2, N'^{(1)}_3, \gamma_1, \gamma_2) &= N'^{(3)}_{122}(N'^{(1)}_1, N'^{(1)}_3, -N'^{(1)}_2, \gamma_1, 1-\gamma_1-\gamma_2), \\
N'^{(3)}_{223}(N'^{(1)}_1, N'^{(1)}_2, N'^{(1)}_3, \gamma_1, \gamma_2) &= N'^{(3)}_{122}(N'^{(1)}_3, N'^{(1)}_2, -N'^{(1)}_1, 1-\gamma_1-\gamma_2, \gamma_2), \\
N'^{(3)}_{233}(N'^{(1)}_1, N'^{(1)}_2, N'^{(1)}_3, \gamma_1, \gamma_2) &= N'^{(3)}_{122}(N'^{(1)}_2, N'^{(1)}_3, N'^{(1)}_1, \gamma_2, 1-\gamma_1-\gamma_2).
\end{aligned} \tag{32}$$

The optimization problem for entropy maximization given by Eq. (15) cannot be solved on directly everywhere on the boundaries of the realizability domain $\mathcal{R}^2_T$, denoted as $\partial\mathcal{R}^2_T$, as the corresponding entropy maximizing distribution can become singular due to the fact that propagation of radiation is then only allowed along specific directions or becomes planar, instead of spanning the full solid angle. In these situations, the intensity distribution is either uniquely determined by a Dirac delta distribution or a combination of Dirac delta distributions, or an entropy maximizing distribution describing propagation of radiation on the (unit) circle as discussed in Appendix B. Pre-computed values of $N^{(3)}$ can then be obtained by solving the appropriate optimization problem for entropy maximization in the interior of $\mathcal{R}^2_T$ and in regions of $\partial\mathcal{R}^2_T$ where exact analytical expressions for $N^{(3)}$ are not available.

Based on the interpolation used to prove sufficiency of the conditions for moment realizability up to second-order and the known exact analytical form of $N'^{(3)}_{111}$, $N'^{(3)}_{122}$, $N'^{(3)}_{123}$ on the boundaries of $\mathcal{R}^2_T$ (see Table 1), the following approximations are proposed:

$$N'^{(3)}_{111}(\|N'^{(1)}\|, \theta, \phi, \gamma_1, \gamma_2) = N'^{(1)}_1\left[\left(N'^{(1)}_1\right)^2 + f_{N'^{(3)}_{111}}(1 - \|N'^{(1)}\|^2)\right], \tag{33}$$

$$N'^{(3)}_{122}(\|N'^{(1)}\|, \theta, \phi, \gamma_1, \gamma_2) = N'^{(1)}_1\left[\left(N'^{(1)}_2\right)^2 + f_{N'^{(3)}_{122}}(1 - \|N'^{(1)}\|^2)\right], \tag{34}$$

$$N'^{(3)}_{123}(\|N'^{(1)}\|, \theta, \phi, \gamma_1, \gamma_2) = f_{N'^{(3)}_{123}} N'^{(1)}_1 N'^{(1)}_2 N'^{(1)}_3, \tag{35}$$

where θ and ϕ, respectively represent the polar and azimuthal angles characterizing the direction of the first-order normalized moment, $N'^{(1)}$, in a spherical coordinate system and are defined as follows

$$\theta = \arccos\left(\frac{N'^{(1)}_3}{\|N'^{(1)}\|}\right), \quad \phi = \arccos\left(\frac{N'^{(1)}_1}{\sqrt{\left(N'^{(1)}_1\right)^2 + \left(N'^{(1)}_2\right)^2}}\right), \tag{36}$$

and $f_{N'^{(3)}_{111}} = f_{N'^{(3)}_{111}}(\|N'^{(1)}\|, \theta, \phi, \gamma_1, \gamma_2)$, $f_{N'^{(3)}_{122}} = f_{N'^{(3)}_{122}}(\|N'^{(1)}\|, \theta, \phi, \gamma_1, \gamma_2)$, and $f_{N'^{(3)}_{123}} = f_{N'^{(3)}_{123}}(\|N'^{(1)}\|, \theta, \phi, \gamma_1, \gamma_2)$ are polynomial expressions defined such that the approximations of the closing flux accurately reproduce pre-computed solutions of the optimization problem for entropy maximization. For illustration purposes, isocontours of $f_{N'^{(3)}_{111}}$, $f_{N'^{(3)}_{122}}$, and $f_{N'^{(3)}_{123}}$, over the triangle $P_1P_2P_3$ are illustrated in Figs. 2(a), (b), and (c), respectively. For accurately approximating the pre-computed solutions as well as derivatives on the boundaries of the realizable space, we choose to write $f_{N'^{(3)}_{111}}$, $f_{N'^{(3)}_{122}}$, and $f_{N'^{(3)}_{123}}$ as affine combinations of the form

$$f_{N'^{(3)}_{111}}(\|N'^{(1)}\|, \theta, \phi, \gamma_1, \gamma_2) = \gamma_1\left[1 + (1-\gamma_1) g_{N'^{(3)}_{111}}\right], \tag{37}$$

$$f_{N'^{(3)}_{122}}(\|N'^{(1)}\|, \theta, \phi, \gamma_1, \gamma_2) = \gamma_2\left[1 + \gamma_1 g_{N'^{(3)}_{122}}\right], \tag{38}$$

$$f_{N'^{(3)}_{123}}(\|N'^{(1)}\|, \theta, \phi, \gamma_1, \gamma_2) = 1 + \gamma_1\gamma_2\gamma_3 g_{N'^{(3)}_{123}}, \tag{39}$$

where $g_{N'^{(3)}_{111}} = g_{N'^{(3)}_{111}}(\|N'^{(1)}\|, \theta, \phi, \gamma_1, \gamma_2)$, $g_{N'^{(3)}_{122}} = g_{N'^{(3)}_{122}}(\|N'^{(1)}\|, \theta, \phi, \gamma_1, \gamma_2)$, and $g_{N'^{(3)}_{123}} = g_{N'^{(3)}_{123}}(\|N'^{(1)}\|, \theta, \phi, \gamma_1, \gamma_2)$ are polynomial expressions which are written as series expansion in terms of orthogonal basis functions as follows

$$g_{N'^{(3)}_{111}} = \sum_{i=0}^{n_i}\sum_{j=0}^{n_j}\sum_{k=-j}^{j}\sum_{l=0}^{n_l}\sum_{m=0}^{n_m} C^{N'^{(3)}_{111}}_{ijklm} T_{2i}(\|N'^{(1)}\|) Y^k_j(\theta, \phi) T_l(\hat{\gamma}_1) T_m(\hat{\gamma}_2), \tag{40}$$

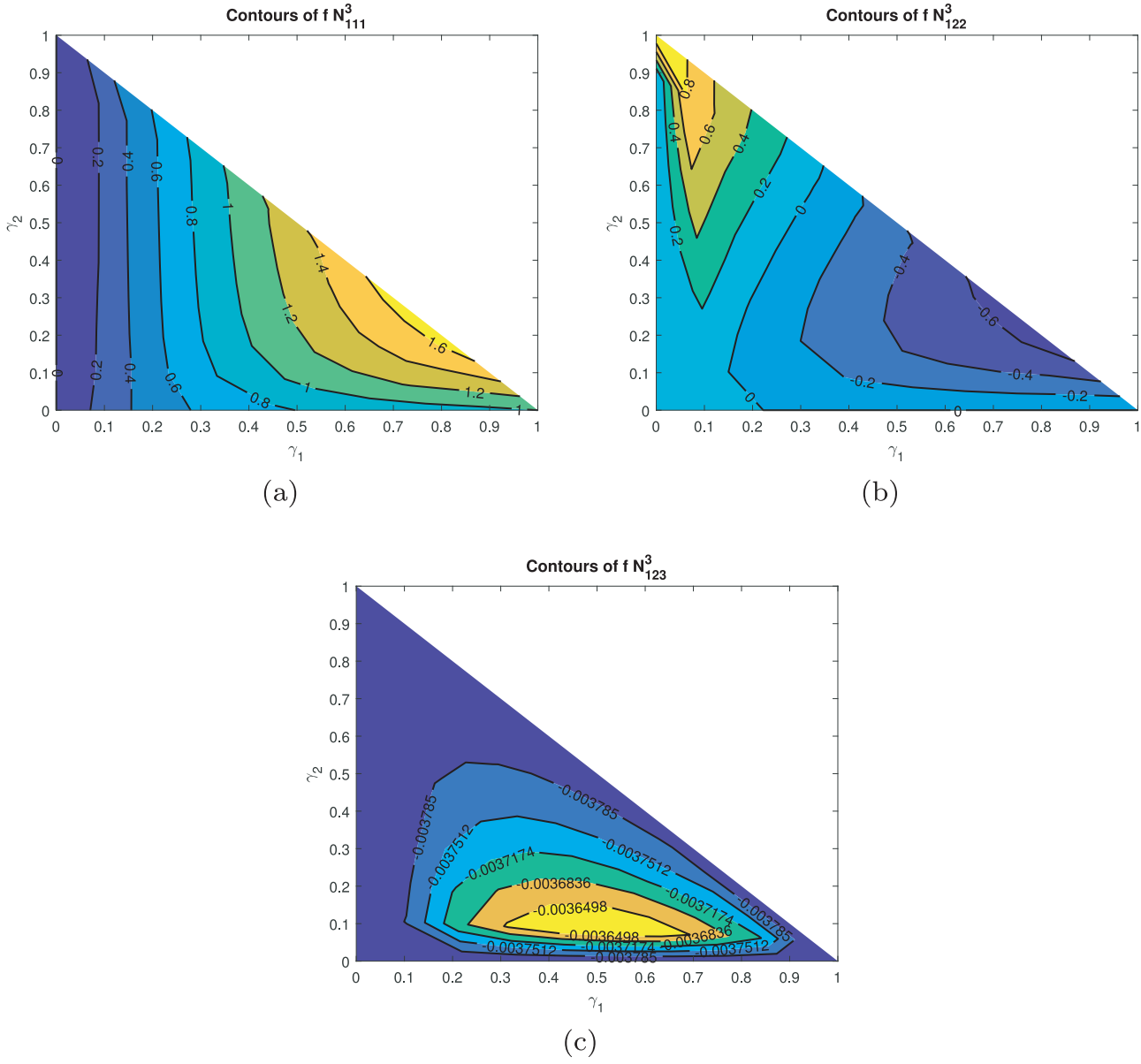

Fig. 2. Isocontours of (a) $f_{N^3_{111}}$; (b) $f_{N^3_{122}}$ and (c) $f_{N^3_{123}}$ over the triangle $P_1P_2P_3$ for $N'^{(1)}_1 = 0.4$, $N'^{(1)}_2 = 0.2$, $N'^{(1)}_3 = 0.15$.

$$g_{N'^{(3)}_{122}} = \sum_{i=0}^{n_i}\sum_{j=0}^{n_j}\sum_{k=-j}^{j}\sum_{l=0}^{n_l}\sum_{m=0}^{n_m} C^{N'^{(3)}_{122}}_{ijklm} T_{2i}(\| N'^{(1)} \|) Y^k_j(\theta,\phi) T_l(\hat{\gamma}_1) T_m(\hat{\gamma}_2), \tag{41}$$

$$g_{N^{(3)}_{123}} = \sum_{i=0}^{n_i}\sum_{j=0}^{n_j}\sum_{k=-j}^{j}\sum_{l=0}^{n_l}\sum_{m=0}^{n_m} C^{N'^{(3)}_{123}}_{ijklm} T_{2i}(\| N'^{(1)} \|) Y^k_j(\theta,\phi) T_l(\hat{\gamma}_1) T_m(\hat{\gamma}_2), \tag{42}$$

where $\hat{\gamma}_1$ and $\hat{\gamma}_2$ are obtained through a rectangle-triangle mapping of the form

$$\gamma_1 = \frac{1+\hat{\gamma}_1}{2}\frac{2-(1-\zeta)(1+\hat{\gamma}_2)}{2}, \qquad \gamma_2 = \frac{1+\hat{\gamma}_2}{2}\frac{2-\zeta(1+\hat{\gamma}_1)}{2}, \tag{43}$$

and where ζ is a parameter for the mapping. In Eqs. (40), (41), and (42), T_n is a Chebyshev polynomial of the first kind of order n, Y^k_j is a spherical harmonic function of degree j and order k, and $C^{N'^{(3)}_{111}}_{ijklm}$, $C^{N'^{(3)}_{122}}_{ijklm}$, as well as $C^{N'^{(3)}_{123}}_{ijklm}$, $i = 0,\ldots,n_i$, $j = 0,\ldots,n_j$, $k = -j,\ldots,j$, $l = 0,\ldots,n_l$, $m = 0,\ldots,n_m$ are coefficients to be determined such that the proposed approximation of the M_2 closure accurately reproduces pre-computed solutions of the optimization problem for entropy maximization for sets of moments up to second-order spanning the full realizable space. The coefficients of the interpolant are computed by solving the Vandermonde system arising from the enforcement of Eqs. (40), (41), and (42) at various nodal points throughout the realizable space. Following a careful analysis of the numerical solutions of the optimization problem for entropy maximization, the interpolation points for $\|N'^{(1)}\|$, $\hat{\gamma}_1$, and $\hat{\gamma}_2$ were chosen to coincide with roots of Chebyshev polynomials of order $2n_i$, n_l, and n_m, respectively, for given values of n_i, n_l, and n_m. On the other hand, the interpolation nodes for θ were selected to correspond to roots of the Legendre polynomials of order n_j and a set of $2n_j$ points uniformly distributed on the unit circle are chosen for ϕ. In order to assess the accuracy of the proposed interpolative-based approximation of the M_2 closure, its val-

ues, obtained by evaluating the approximations at a relatively large number of points uniformly distributed throughout the realizable domain, were compared to solutions of the entropy maximization problem at the points of interest. More specifically, a set of 50 values of each of the variables $\|N^{(1)}\|$, θ, ϕ, equally distributed in $[0,1]$, $[0,\pi]$ and $[0,2\pi]$, respectively, as well as 20 values of $\hat{\gamma_1}$ and of $\hat{\gamma_2}$ equally distributed within the triangle (P_1, P_2, P_3) as depicted in Fig. 1, were considered in the validation of the proposed interpolant. The choices for the optimal number of coefficients, n_i, n_j, and n_l, were dictated by the convergence of the preceding approximations to the computed maximum-entropy solution in both the L^2- and L^∞-norm sense.

4.3. Numerical solution of the optimization problem for entropy maximization

The entropy of radiation based on Bose-Einstein statistics given by Eq. (10) is a strictly convex functional, and, as such, any locally optimal set of Lagrange multipliers, α, would also be a globally optimal set. The sequential quadratic programming (SQP) algorithm, as implemented in the software package NLopt [37–39] an open source library for nonlinear optimization, was therefore used for the solution of the optimization problem as defined by Eq. (11). In this implementation, an objective function and its gradients, as well as additional constraints, are supplied by the user. The Hessian matrix of second derivatives, which is required for solving the Newton system of equations, is then estimated by means of the Broyden-Fletcher-Goldfarb-Shanno (BFGS) algorithm, which provides substantial computational savings compared to the direct evaluation of the Hessian matrix. The algorithm provides very good convergence for sets of moments far away from the boundaries of the realizability domain. However, as one of the boundaries is approached, the dual optimization problem becomes increasingly difficult to solve and might even fail to converge due to ill-conditioning of the Hessian matrix. In order to improve the condition number of the Hessian matrix, a preconditioning of the latter, similar to that described by Alldredge et al. [40] is advocated. The preconditioning is equivalent to an adaptive change of polynomial basis, relative to the original basis $\boldsymbol{m}(\vec{s})$, such that the Hessian is the identity matrix in the new basis. In addition, the regularization scheme introduced by Alldredge et al. [41] is employed to make the optimization algorithm more robust, especially for very ill-conditioned problem. Instead of using a Cholesky factorization of the Hessian for the preconditioning as chosen by Alldredge et al. [40], the numerically stable modified Gram-Schmidt algorithm, described by Abramov [42], is adopted. Furthermore, instead of preconditioning the Hessian matrix at each Newton step during the optimization, the procedure developed by Abramov [43], allowing for several Newton steps between successive reorthogonalizations, is adopted. The procedure consists of tracking the condition number of the inverse of the Hessian during the BFGS iterations, and then precondition the Hessian matrix whenever the condition number exceeds a threshold value of 20.

5. Boundary conditions

The numerical solution of systems of partial differential equations generally requires the prescription of boundary conditions in order to evaluate the numerical fluxes at the boundaries of the computational domain. In the context of the system of equations for the angular moments of the radiative intensity distribution resulting from moment closures, boundary conditions are generally prescribed in terms of the full moments. However, only the outgoing partial moments are generally known at a given boundary. In this work, boundary conditions are prescribed using a partial moment approach in which the boundary data is viewed as a sum of the two contributions: one from the radiation that is incoming to the boundary and one from the outgoing radiation. The latter is obtained by taking angular integrals of the outgoing distribution of radiative intensity, which, in the case of diffusively reflecting and emitting wall surfaces, as is the case in most practical combustion systems [44], can be expressed as follows

$$I_w = \epsilon_w I_b(T_w) + \frac{(1-\epsilon_w)}{\pi} \int_{\Omega=2\pi} s(i) I \mathrm{d}\Omega, \tag{44}$$

where T_w and ϵ_w represent the wall temperature and emissivity, respectively. The derivation of the partial outgoing moments is straightforward for black walls ($\epsilon_w = 1$). However, if the walls also reflect a portion of the incoming radiation, the derivation of the outgoing partial moments can be quite challenging, especially for entropy-maximizing distributions for which analytical integrals of the underlying intensity distribution cannot be obtained. For the P_N approximations, the partial outgoing moments can directly be expressed in terms of the moments of the distribution.

In order to prescribe values for the full moments, the partial incoming moments, which depend on the incoming intensity, must also be specified at the boundaries. Closed form analytical expressions for the partial incoming moments in terms of the incoming full moments exist for the P_N moment closure, but not for the M_N maximum-entropy closures. For the latter, the optimization problem for entropy maximization can again be solved repeatedly whenever boundary conditions are required. Such a procedure is adopted for the M_2 closure here; however, in order to eliminate the relatively high computational costs that are associated with the numerical presciption of the boundary data, interpolative-based analytical approximations of the incoming partial moments have been developed for the M_1 closure in the context of radiative transfer in gray participating media, and will be described in a future follow-on paper. The construction of similar types of approximations of the incoming partial moments for the M_2 closure will be the subject of other future studies. Note that the partial moment approach adopted herein is fully consistent and by construction the boundary conditions will yield the appropriate full moments for the case of identical incoming and outgoing radiation intensity distributions.

5.1. Partial moments for gray M_2 closure

Similar to the closing fluxes for the M_2 maximum-entropy closure, closed-form analytical expressions do not exist for the partial moments of the M_2 model and they must in general be evaluated numerically. While it would seem possible to formulate accurate and efficient interpolative-based approximations to the partial moments similar to those developed herein for the M_2 closing fluxes, this was deemed beyond the scope of the present study. Instead, the incoming partial moments for the gray M_2 closure are obtained by numerically solving the dual optimization problem for entropy maximization, Eq. (15), for any given realizable set of moments up to second-order. The SQP algorithm outlined in Section 4.3 above is again used in the solution of the optimization problem. The associated entropy maximizing distribution with known Lagrange multipliers, which takes the form given in Eq. (14), can then be integrated over the appropriate half space to obtain the partial moments of interest. This numerical approach, despite being relatively computationally expensive, represents a first step in the development of partial moment boundary conditions for the M_2 closure and permits the assessment of the predictive capabilities of the proposed interpolative-based M_2 closure as considered here. The development of accurate and more efficient interpolative-based approximations of the partial moment boundary data will be the subject of future follow-on research.

5.2. Partial moments for gray M_1 closure

Despite the existence of a closed form analytical expression for the gray first-order maximum-entropy, M_1, closure, there also exists no exact analytical expression for the corresponding partial moments in multiple space dimensions. As for the M_2 closure, the incoming partial moments for the gray M_1 closure could also be obtained by numerically solving the dual optimization problem for entropy maximization; however, in this study, the partial moments needed for prescribing the boundary data were obtained using interpolative-based analytical approximations of the numerically-evaluated partial moments. The proposed interpolants for the partial moments of the gray M_1 closure are defined such that analytical expressions in both the isotropic and free-streaming limits are exactly reproduced, and pre-computed solutions of the optimization problem for entropy maximization, for sets of moments spanning the full realizable space for moments up to first-order, are accurately approximated. Due to length restrictions, the interpolative-based expressions for the partial moments are not described herein, but will be the subject of a future follow-on paper.

6. Numerical solution method

Like the P_1, P_3, and M_1 moment closures, the proposed interpolative-based second-order M_2 maximum-entropy moment closure is strictly hyperbolic in the sense of Lax [45]. In the original definition, quasi-linear inhomogeneous PDEs are said to be strictly hyperbolic if the eigenvalues associated with the eigensystem of the coefficient matrices and flux Jacobians are all real and distinct. A slightly less restrictive demand for strict hyperbolicity is that the eigenvalues are all real (i.e., repeated eigenvalues are permitted) and that the corresponding right eigenvectors form a complete and linearly independent set such that the coefficient matrices and flux Jacobians are diagonizable. Levermore [46] has shown that the maximum-entropy closures applied to the Boltzmann equations of gas kinetic theory with the Boltzmann entropy result in moment equations that are symmetric hyperbolic systems and strictly hyperbolic. Quasi-linear hyperbolic PDEs of the type governing the system of angular moments for the M_2 closure are very well suited for solution by the now standard family of upwind finite-volume spatial discretization techniques originally developed by Godunov [47]. In this study, solutions of the proposed interpolative-based M_2 closure for gray media, as well as the P_1, P_3, and M_1 moment closures, are all obtained using a parallel, implicit, upwind Godunov-type finite-volume scheme similar to those previously described by Groth and co-workers [3,31,48–51] for systems of partial differential equations. In what follows, the proposed numerical solution methodology is described for the M_2 moment closure. Similar solution methods are applied here for solution of the other three closure methods. Additionally, the hyperbolicity of the proposed interpolative-based M_2 closure is explored by numerical means and discussed in Subsection 6.2 below.

6.1. Weak conservation form of M_2 moment equations

The finite-volume scheme for the proposed interpolative-based second-order M_2 closure considers the solution of the weak conservation form of the moment equations on two-dimensional, body-fitted, multi-block, quadrilateral meshes. The weak conservation form of the M_2 moment equations for a two-dimensional Cartesian coordinate system can be obtained by taking appropriate angular moments of the underlying RTE for a gray medium and written as

$$\frac{\partial \mathbf{U}}{\partial t}+\frac{\partial \mathbf{F}}{\partial x}+\frac{\partial \mathbf{G}}{\partial y}=\mathbf{S}, \tag{45}$$

where $\mathbf{U}$ is the vector of conserved moments given by

$$\mathbf{U}=\left[I^{(0)},I_x^{(1)},I_y^{(1)},I_{xx}^{(2)},I_{xy}^{(2)},I_{yy}^{(2)}\right]^T, \tag{46}$$

$\mathbf{F}$ and $\mathbf{G}$ are the flux vectors in the x- and y-coordinate directions, respectively, having the form

$$\begin{aligned}\mathbf{F}&=c\left[I_x^{(1)},I_{xx}^{(2)},I_{xy}^{(2)},I_{xxx}^{(3)},I_{xxy}^{(3)},I_{xyy}^{(3)}\right]^T,\\ \mathbf{G}&=c\left[I_y^{(1)},I_{xy}^{(2)},I_{yy}^{(2)},I_{yxx}^{(3)},I_{yxy}^{(3)},I_{yyy}^{(3)}\right]^T,\end{aligned} \tag{47}$$

and where S represents the source term, which, under the assumption of isotropic scattering, is given by

$$\mathbf{S}=c\begin{bmatrix}\kappa\left(aT^4-I^{(0)}\right)\\ -(\kappa+\sigma_s)I_x^{(1)}\\ -(\kappa+\sigma_s)I_y^{(1)}\\ \frac{1}{3}\left(\kappa aT^4+\sigma_sI^{(0)}\right)-(\kappa+\sigma)I_{xx}^{(2)}\\ -(\kappa+\sigma)I_{xy}^{(2)}\\ \frac{1}{3}\left(\kappa aT^4+\sigma_sI^{(0)}\right)-(\kappa+\sigma)I_{yy}^{(2)}\end{bmatrix}. \tag{48}$$

In Eqs. (45)–(48), the third-order moment fluxes are expressed in terms of the lower-order moments using Eqs. (33), (34), (35), and (32) defined above, thereby resulting in the gray M_2 closure.

Although not shown here, due to the hierarchical structure of the equations for the angular moments given in Eq. (45), it is relatively straightforward to apply a perturbative analysis and show that the M_2 closure formally recovers the usual optically-thick isotropic or so-called diffusion limit [1] commonly encountered in some applications of radiative transfer.

6.2. Hyperbolicity of interpolative-based M_2 moment closure

The hyperbolicity of the proposed interpolative-based M_2 moment closure for two space dimensions is investigated by considering the eigenvalues of the flux Jacobian $\mathbf{A}=\partial\mathbf{F}/\partial\mathbf{U}$ and $\mathbf{B}=\partial\mathbf{G}/\partial\mathbf{U}$ for the x- and y-coordinate directions, respectively. Hyperbolicity is ensured if the eigenvalues of the Jacobians $\mathbf{A}$ and $\mathbf{B}$ are all real. For the M_2 closure, the flux Jacobian in the x-direction, $\mathbf{A}$, can be written as

$$\mathrm{A}=\frac{\partial \mathrm{F}}{\partial \mathrm{U}}=c\begin{bmatrix}0&1&0&0&0&0\\ 0&0&0&1&0&0\\ 0&0&0&0&1&0\\ \frac{\partial I_{xxx}^{(3)}}{\partial I^{(0)}}&\frac{\partial I_{xxx}^{(3)}}{\partial I_x^{(1)}}&\frac{\partial I_{xxx}^{(3)}}{\partial I_y^{(1)}}&\frac{\partial I_{xxx}^{(3)}}{\partial I_{xx}^{(2)}}&\frac{\partial I_{xxx}^{(3)}}{\partial I_{xy}^{(2)}}&\frac{\partial I_{xxx}^{(3)}}{\partial I_{yy}^{(2)}}\\ \frac{\partial I_{xxy}^{(3)}}{\partial I^{(0)}}&\frac{\partial I_{xxy}^{(3)}}{\partial I_x^{(1)}}&\frac{\partial I_{xxy}^{(3)}}{\partial I_y^{(1)}}&\frac{\partial I_{xxy}^{(3)}}{\partial I_{xx}^{(2)}}&\frac{\partial I_{xxy}^{(3)}}{\partial I_{xy}^{(2)}}&\frac{\partial I_{xxy}^{(3)}}{\partial I_{yy}^{(2)}}\\ \frac{\partial I_{xyy}^{(3)}}{\partial I^{(0)}}&\frac{\partial I_{xyy}^{(3)}}{\partial I_x^{(1)}}&\frac{\partial I_{xyy}^{(3)}}{\partial I_y^{(1)}}&\frac{\partial I_{xyy}^{(3)}}{\partial I_{xx}^{(2)}}&\frac{\partial I_{xyy}^{(3)}}{\partial I_{xy}^{(2)}}&\frac{\partial I_{xyy}^{(3)}}{\partial I_{yy}^{(2)}}\end{bmatrix}, \tag{49}$$

where the derivatives of the closing fluxes with respect to the lower-order moments making up the components of the solution vector, $\mathbf{U}$, in $\mathcal{R}^2$, can be written in the form

$$\frac{\partial I_{ijk}^{(3)}}{\partial U_q}=I'^{(3)}_{lmn}\frac{\partial}{\partial U_q}\left(R_{li}R_{mj}R_{nk}\right)+R_{li}R_{mj}R_{nk}\frac{\partial I'^{(3)}_{lmn}}{\partial U_q}, \tag{50}$$

where

$$\frac{\partial I'^{(3)}_{ijk}}{\partial U_q}=\frac{\partial I'^{(3)}_{lmn}}{\partial U'_q}\left[R_{ij}(\mathbf{U})\delta_{jq}+U_j\frac{\partial R_{ij}(\mathbf{U})}{\partial U_q}\right], \tag{51}$$

and where

$$\frac{\partial}{\partial U_q}\left(R_{li}R_{mj}R_{nk}\right)=R_{mj}R_{nk}\frac{\partial R_{li}}{\partial U_q}+R_{li}R_{nk}\frac{\partial R_{mj}}{\partial U_q}+R_{li}R_{mj}\frac{\partial R_{nk}}{\partial U_q}. \tag{52}$$

Analytical expressions of the derivatives for the closing fluxes $I'^{(3)}_{ijk}$, in $\mathcal{R}^2_T$, with respect to the lower-order moments, U'_q, in $\mathcal{R}^2_T$, can be readily derived by using Eqs. (33), (34), (35) and (32). Furthermore, the derivatives appearing in Eq. (52) can also be obtained

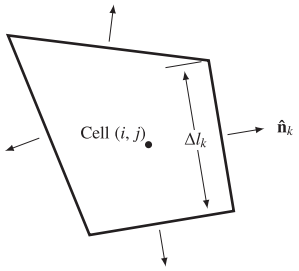

Fig. 3. Quadrilateral computational cell of two-dimensional multi-block body-fitted mesh.

from the analytical form of the rotation matrix, R, with respect to the lower-order moments, U_q, in $\mathcal{R}^2$.

The eigenvalues of the x-direction flux Jacobian, $\mathbf{A}$, of Eq. (49) were evaluated numerically for sets of moments spanning the whole realizability domain, $\mathcal{R}^2$. More specifically, 50 values of $\|N^{(1)}\|$ equally distributed in $[0,1]$, 50 of θ equally distributed in $[0,\pi]$, 50 of ϕ equally distributed in $[0,2\pi]$, and 100 sets of values of $(\gamma_1, \gamma_2, \gamma_3)$ equally distributed within the associated equilateral triangle, were used for the investigation of hyperbolicity. The numerical study revealed that the eigenvalues of the flux Jacobian, $\mathbf{A}$, are all real valued for all of the points considered within the space of realizable moments. Due to the geometric symmetries of the closure, similar findings are expected for the y-direction flux Jacobian, $\mathbf{B}$. While the numerical tests are certainly not a proof that the eigenvalues are everywhere real nor was the issue of strict hyperbolicity tested as part of this study as it was felt that the distinct nature of the eigenvalues and/or non-degenerate nature of the eigenstructure can be difficult to confirm by numerical means, the local hyperbolicity of the proposed interpolative-based closure for all points examined within the space of physically realizable moments is very encouraging and provides strong evidence of the extent to which the proposed interpolative-based closure mimics the actual M_2 maximum-entropy model.

6.3. Finite-volume spatial discretization procedure and semi-discrete form

In the proposed second-order limited upwind finite-volume method, the integral form of the conservation equations defined by Eq. (45) are applied to quadrilateral cells of a two-dimensional multi-block body-fitted grid. This results in the so-called semi-discrete form, a coupled system of nonlinear ordinary differential equations for cell-averaged solution quantities which can be written for computational cell (i, j) (see Fig. 3) as

$$\frac{\mathrm{d}\mathbf{U}_{i,j}}{\mathrm{d}t} = -\frac{1}{A_{i,j}} \sum_{m=1}^{N_f} \vec{\mathbf{F}}_{i,j,m} \cdot \vec{n}_{i,j,m}\, \Delta l_{i,j,m} + \mathbf{S}_{i,j}(\mathbf{U}_{i,j}) = -\mathbf{R}_{i,j}(\mathbf{U}), \quad (53)$$

where $\mathbf{U}_{ij} = (1/A_{ij}) \int_{A_{ij}} \mathbf{U} dA$ is the cell-averaged conserved solution vector, $\vec{\mathbf{F}} = [\mathbf{F}, \mathbf{G}]$ is the moment flux vector, $\mathbf{R}_{i,j}(\mathbf{U})$ is the residual vector, A_{ij} is the cell surface area, $\Delta l_{i,j,m}$ and $\vec{n}_{i,j,m}$ are the length and unit outward normal vector of the m^{th} face of quadrilateral cell (i, j) having $N_f = 4$ cell faces, respectively.

6.4. Numerical flux evaluation

The numerical moment flux, $\vec{\mathbf{F}} \cdot \vec{n}$, at cell faces (i, j, m) appearing in the semi-discrete form of the moment equations given in Eq. (53) above are evaluated here using a Riemann solver-based flux function in conjunction with piecewise limited linear reconstruction. In this approach, the numerical moment flux can be expressed as

$$\vec{\mathbf{F}} \cdot \vec{n} = \mathcal{F}(\mathbf{U}_L, \mathbf{U}_R, \vec{n}), \quad (54)$$

where $\mathcal{F}$ is the so-called numerical flux function and $\mathbf{U}_L$ and $\mathbf{U}_R$ are the values of solution at the mid-point of the cell face to the left (inside the cell) and right (outside the cell) of the interface. The widely-used HLLE approximate Riemann solver, based on the approximate Riemann solver of Harten, Lax, and van Leer [52] with estimates of the wave speeds due to Einfeldt [53] is used here to define the flux function, $\mathcal{F}$. Piecewise limited linear reconstruction based on the least-squares approach of Barth [54] with the slope limiter of Venkatakrishnan [55] to ensure solution monotonicity are used to reconstruct the values of $\mathbf{U}_L$ and $\mathbf{U}_R$ at the cell interfaces. Estimates of the fastest and slowest waves speeds needed for the HLLE flux function were approximated by c and $-c$, respectively, where c is the speed of light.

6.5. Block-based anisotropic adaptive mesh refinement (AMR)

While not applied in the present study, the finite-volume scheme described above can be used in conjunction with a block-based hierarchical data structure to facilitate automatic solution-directed mesh adaptation on multi-block mesh according to physics-based criteria. The block-based anisotropic AMR implemented here is similar to that described by Groth and co-workers [56–59] for computations of two-dimensional problems and [57,59–61] for three-dimensional flows. The anisotropic approach allows the adaptation of the mesh based on solution-dependent physics-based criteria as the computation is performed such that areas associated with small spatial scales (e.g., regions with shock, steep gradients, and/or discontinuities) are resolved with appropriately higher mesh densities, while areas with larger spatial scales are resolved on coaser meshes with having large cell sizes. The block-based anisotropic AMR scheme has been shown to be very effective in reducing the overall mesh size for a given flow problem as well as providing efficient and highly scalable implementation on high-performance parallel computing systems using domain decomposition [50,59,61,62].

6.6. Newton krylov schwarz (NKS) method

In most practical applications involving radiative heat transfer, the time scales for the transport of the radiation are generally much smaller than those of the other phenomena involved. As such, steady state solutions of the RTE are of primary interest. Newton's method is applied herein to obtain in an efficient manner steady-state solutions of the algebraic non-linear equations following from Eq. (53) satisfying

$$\mathbf{R}(\mathbf{U}) = -\frac{\mathrm{d}\mathbf{U}}{\mathrm{d}t} = \mathbf{0}. \quad (55)$$

The particular implementation of the Newton method used here has been developed previously by Groth and Northrup [63] as well as Charest et al. [3,64] for computations on large multi-processor parallel clusters. It consists of a Jacobian-free inexact Newton method coupled with an iterative Krylov subspace linear solver. The widely-used generalized minimal residual (GMRES) technique developed by Saad and co-workers [65–68] is used to solve the linear system at each Newton step. The technique is particularly attractive because the left-hand-side matrix of the linear system is not explicitly formed and instead only the results of matrix-vector products are required at each iteration, significantly reducing the required storage. A combination of additive Schwarz and block incomplete lower-upper (BILU) local preconditioning of the linear system is used to ensure effectiveness of the GMRES method. The additive Schwarz preconditioning is easily implemented within

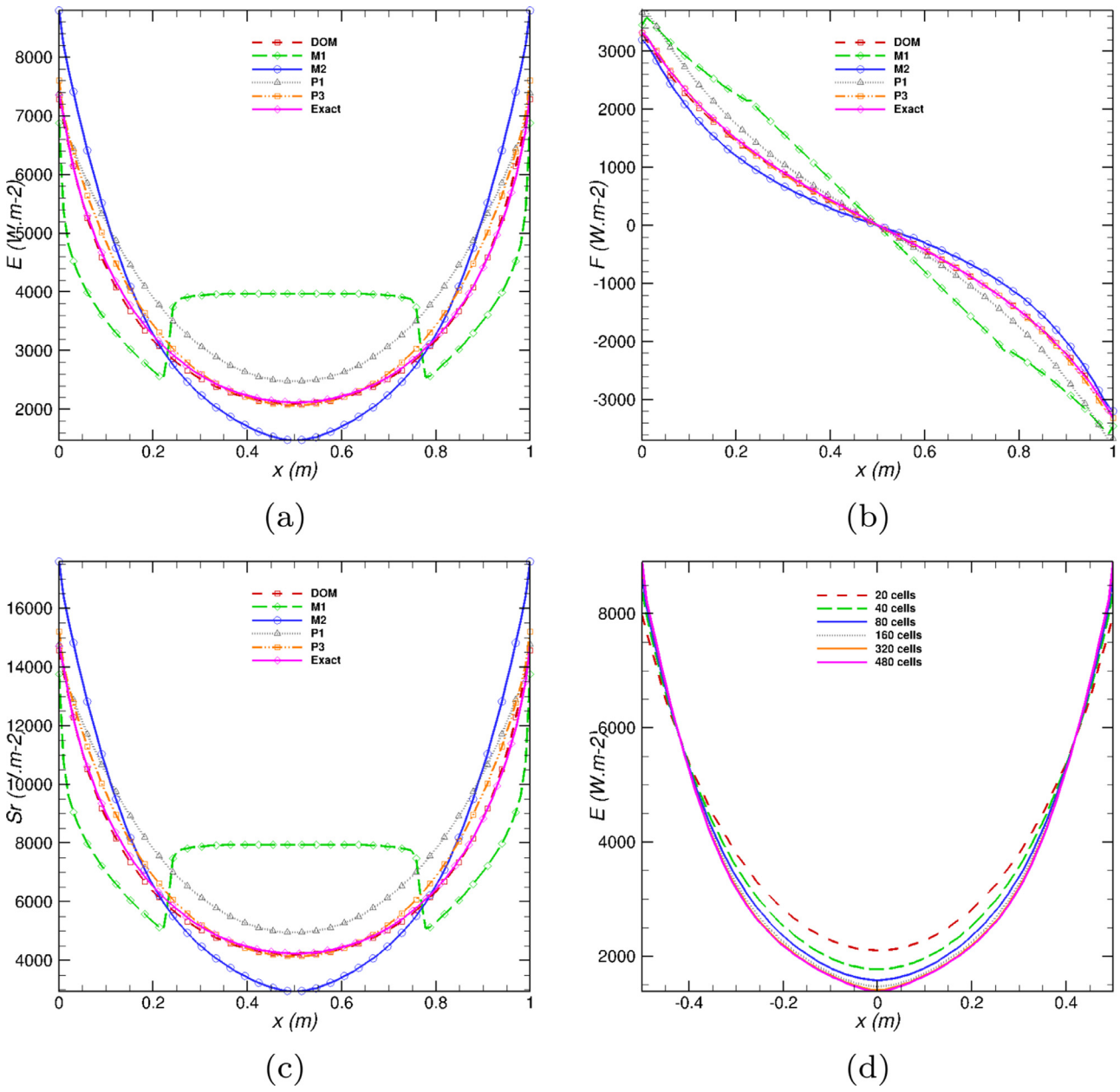

Fig. 4. Radiative transfer between two infinitely long parallel plates with a separation distance of 1m in a cold ($T = 0$K) non-scattering medium showing numerical predictions of (a) the radiative energy, E; (b) radiative flux, F; and (c) the source of radiative energy transfer, S_r, obtained using the M_2 interpolative-based closure using a 320-node mesh compared to the exact analytical solution as well as the predictions of the M_1 maximum-entropy closure, P_1 and P_3 spherical harmonic closures, and DOM; as well as (d) the convergence of the M_2 interpolative-based closure predictions of the radiative energy for varying mesh sizes.

the block-based anisotropic AMR scheme presented in the previous subsection. Finally, to improve the global convergence of the Newton algorithm, an implicit Euler time-marching startup procedure with switched evolution/relaxation (SER) as proposed by Mulder and Van Leer [69] is also applied.

7. Numerical results for gray media

In this section, the predictive capabilities and accuracy of the proposed interpolative-based second-order M_2 maximum-entropy moment closure are compared to and evaluated against the M_1 maximum entropy closure, the P_1 and P_3 spherical harmonic approximations, as well as the DOM for a number canonical test cases in both one and two space dimensions. For all the cases studied, a gray medium with isotropic scattering ($\Phi(\vec{s}', \vec{s}) = 1$) is assumed. Numerical results for all cases have been obtained for each of the moment closures using the upwind finite-volume method described above. Boundary conditions are prescribed using partial moments as described in Section 5. For the DOM, the space marching method used to obtain numerical results is described by Charest et al. [3]. Unless specified otherwise, the DOM is used with quadrature rules based on the T_4 scheme of Thurgood et al. [24]. In some cases, exact analytical solutions are also used as a reference in the comparisons.

The first set of test cases consists of radiative transfer between two parallel plates of infinite length. These essentially one-dimensional problems are similar to those examined previously by Hauck [16,17]. Different scenarios are considered whereby the properties of the medium (radiative properties and temperature) between those two plates, as well as the distance between the

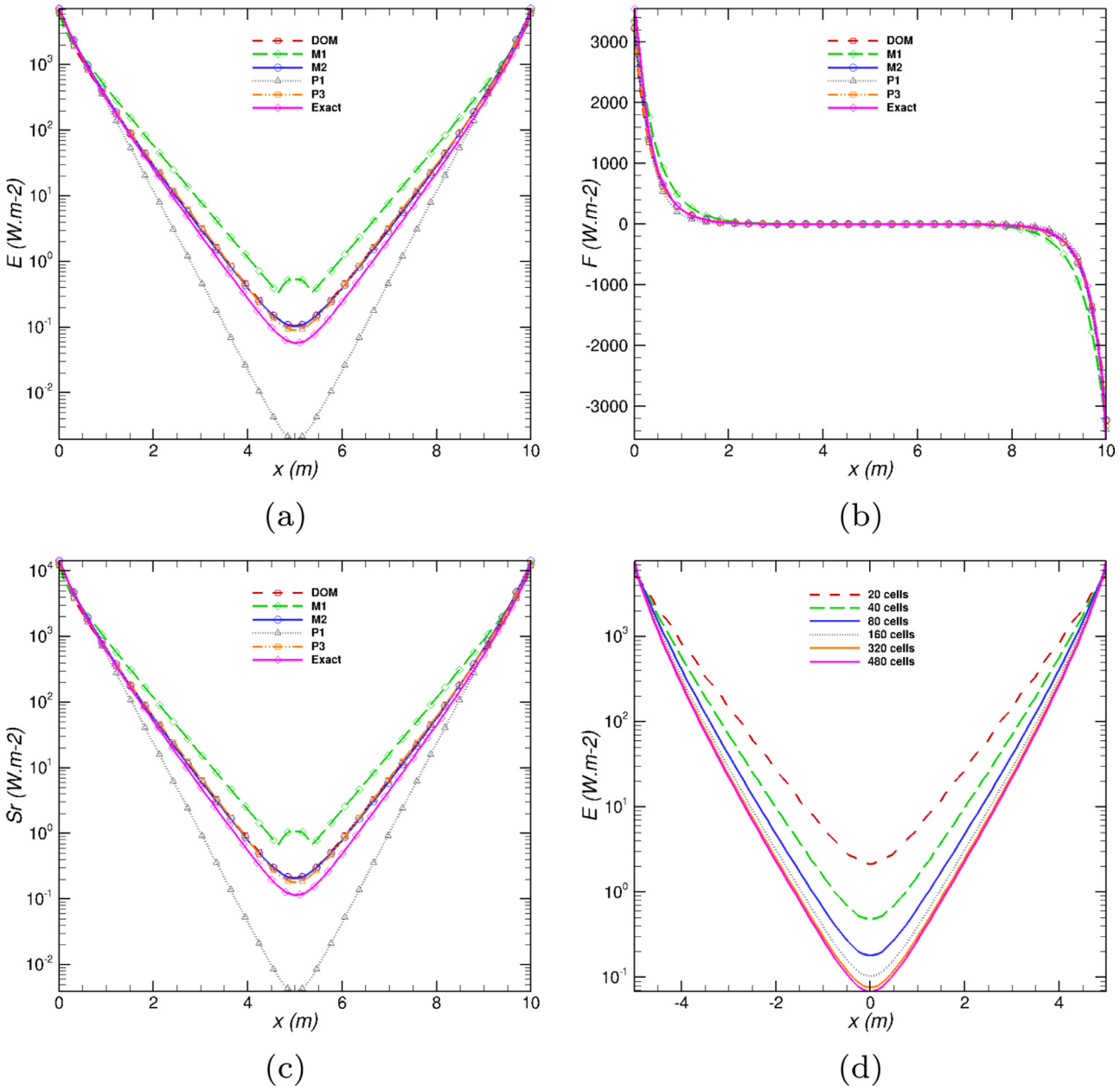

Fig. 5. Radiative transfer between two infinitely long parallel plates with a separation distance of 10m in a cold ($T = 0K$) non-scattering medium showing numerical predictions of (a) the radiative energy, E; (b) radiative flux, F; and (c) the source of radiative energy transfer, S_r, obtained using the M_2 interpolative-based closure using a 320-node mesh compared to the predictions of the M_1 maximum-entropy closure, P_1 and P_3 spherical harmonic closures and DOM; as well as (d) the convergence of the M_2 interpolative-based closure predictions of the radiative energy for varying mesh sizes.

plates, are varied in order to assess the impact on the predictive capabilities of the proposed M_2 closure. The first two-dimensional test case consists of evaluating the accuracy of the M_2 closure in predicting radiative heat transfer throughout a cold (non-emitting) and absorbing medium contained within a square enclosure for which all of the walls have the same temperature. Lastly, a line source problem, which consists of a cold, non-scattering and strongly absorbing medium, confined within a square computational domain, is also considered.

7.1. Parallel plates

As a first assessment of the proposed interpolative-based M_2 closure, radiative transfer between two hot parallel plates of infinite length compared to their separation distance is studied. Two variants of this problem are considered. In the first variant of this test case, the medium between the plates is assumed to be cold (non-emitting) non-scattering, and the predictions of the different radiation models are compared for different plate separation distances. The second variant of this test case considers the effects of scattering on the predictive capabilities of the M_2 interpolative-based closure.

7.1.1. Exact solution for non-scattering case

For a non-scattering medium confined between two black, parallel plates, there exists an exact analytical solution to the radiative transfer equation as given by Modest [1]. The distribution of the radiative intensity emitted from the lower and upper plates are

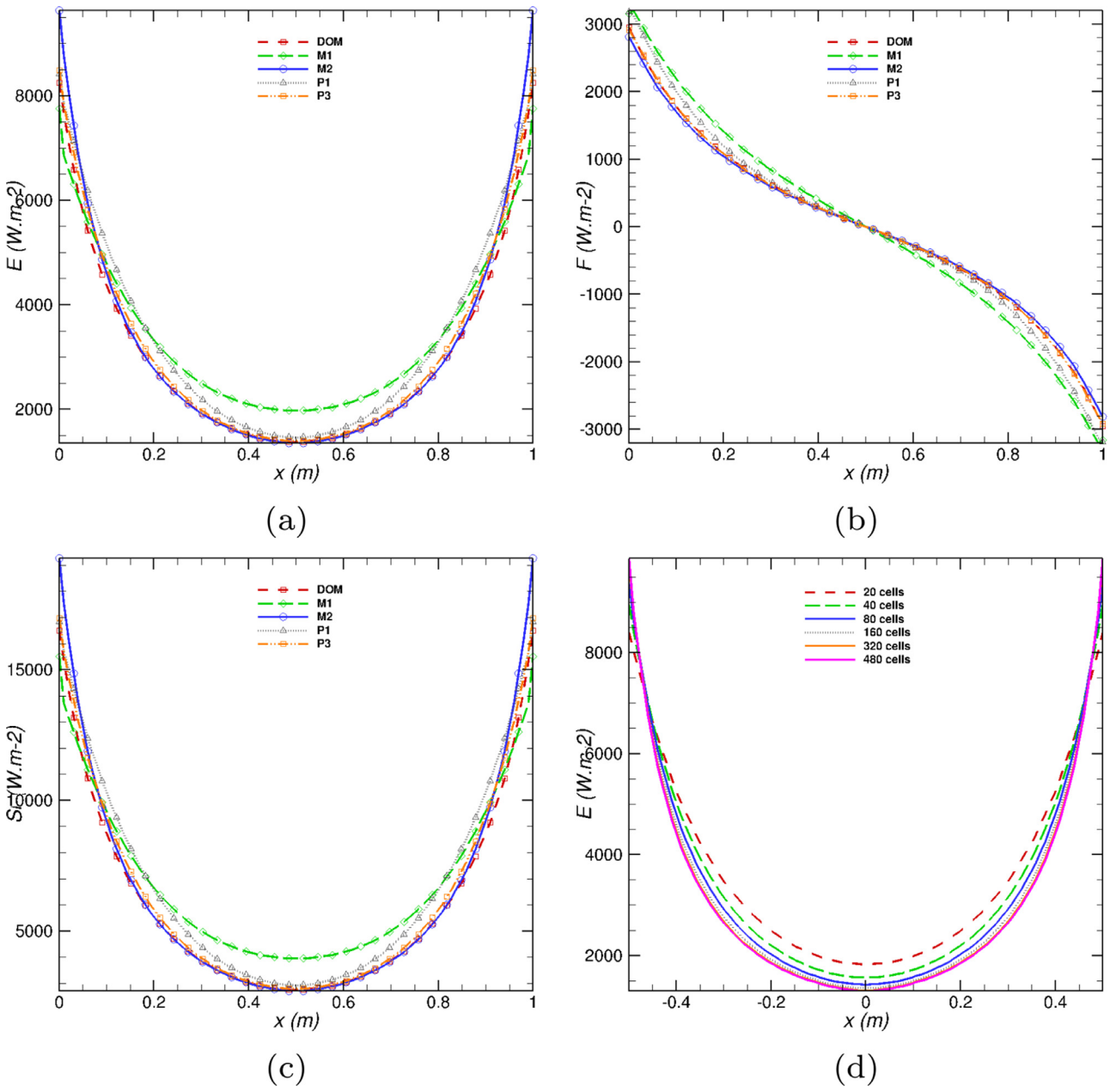

Fig. 6. Radiative transfer between two infinitely long parallel plates with a separation distance of 1m in a cold ($T = 0$K) scattering medium showing numerical predictions of (a) the radiative energy, E; (b) radiative flux, F; and (c) the source of radiative energy transfer, S_r, obtained using the M_2 interpolative-based closure using a 320-node mesh compared to the predictions of the M_1 maximum-entropy closure, P_1 and P_3 spherical harmonic closures and DOM; as well as (d) the convergence of the M_2 interpolative-based closure predictions of the radiative energy for varying mesh sizes.

given by

$$I^+(\tau\prime,\mu) = I_{w1}e^{-\tau/\mu} + \frac{1}{\mu}\int_0^{\tau} I_b(\tau\prime)e^{-(\tau-\tau\prime)/\mu}\mathrm{d}\tau\prime$$
$$= I_b + (I_{w1} - I_b)e^{-\tau/\mu} \qquad 0 < \mu < 1 \tag{56}$$

$$I^-(\tau\prime,\mu) = I_{w2}e^{(\tau_L-\tau)/\mu} - \frac{1}{\mu}\int_0^{\tau} I_b(\tau\prime)e^{(\tau\prime-\tau)/\mu}\mathrm{d}\tau\prime$$
$$= I_b + (I_{w2} - I_b)e^{(\tau_L-\tau)/\mu} \qquad -1 < \mu < 0 \tag{57}$$

respectively, where $\tau_L = \int_0^L \beta(s)ds$ is the optical thickness (or optical depth), L is the distance between the two plates, I_{w1} and I_{w2} are the intensities leaving the lower and upper plates respectively, $I_b(\tau\prime) = I_b$ is the black-body radiative intensity distribution of the medium, and the substitution $\mu = \cos\theta$ is made to simplify the analysis.

Very accurate zeroth and first moments of the preceding exact solutions of the radiative intensities can be achieved by using a 20-point Gauss-Legendre quadrature rule such that

$$E^{\pm} = \pm 2\pi \int_0^{\pm 1} I^{\pm}(\tau,\mu)\mathrm{d}\mu = 2\pi \sum_{n=1}^{20} w_n I^{\pm}(\tau,\mu_n) \tag{58}$$

$$F^{\pm} = \pm 2\pi \int_0^{\pm 1} \mu I^{\pm}(\tau,\mu)\mathrm{d}\mu = 2\pi \sum_{n=1}^{20} w_n \mu_n I^{\pm}(\tau,\mu_n) \tag{59}$$

where the points μ_n and weights w_n are determined by the Gauss-Legendre quadrature in the appropriate domains (i.e., $\mu_n \in [0, 1]$ for lower plate and $\mu_n \in [-1, 0]$ for upper plate). The overall ra-

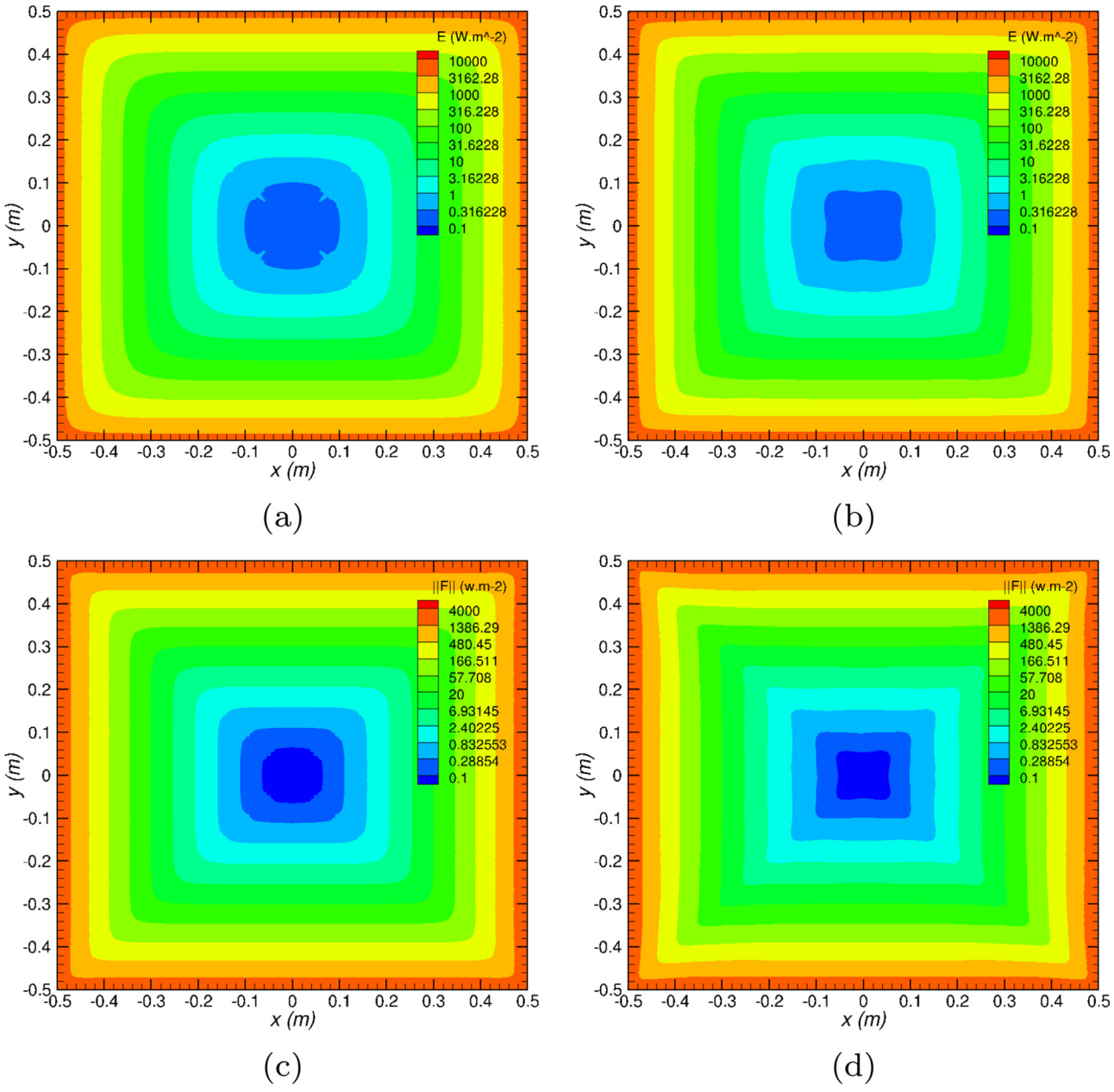

Fig. 7. Radiative transfer within square enclosure containing cold (non-emitting) and absorbing medium with wall temperatures of $T = 500$K showing numerical predictions of the distribution of the radiative energy density using (a) the DOM & (b) the interpolative-based M_2 moment closure; the distribution of the magnitude of the radiative energy flux as obtained using (c) the DOM & (d) our interpolative-based M_2 moment closure, on a (320 × 320)-node mesh.

diative energy at any optical distance, τ, between the two plates is the sum of the radiative energy arising from both the lower and upper plates. This sum also holds true for the overall radiative heat flux.

7.1.2. Cold medium with no scattering

As a first test case, radiative transfer throughout a cold ($T = 0$K), non-scattering medium with an absorption coefficient $\kappa = 2\text{m}^{-1}$ between two parallel plates was studied. Each of the plates was taken to have a temperature of $T = 500$K. The predictions for the radiative energy density, radiative heat flux, and radiative source term obtained using the proposed M_2 interpolative-based closure as well as the M_1, P_1 and P_3 moment closures and DOM are compared for two plate separation distances: 1 and 10m as shown in Figs. 4 and 5, respectively. The predictions in all cases were obtained using 320-node, uniformly-spaced, computational mesh to discretize the space between the two plates. Convergence of the interpolative-based M_2 closure solutions with increasing mesh resolution ranging from 20- to 480-node computational meshes are depicted in Figs. 4(d) and 5(d), confirming that the solutions are satisfactorily converged on the 320-node grid. The analytical solution derived in Eqs. (58) and (59), is used as a reference for the comparisons. Note that for both separation distances, the DOM is observed to agree very closely with the exact solution.

For the small plate separation, it is readily apparent from Fig. 4 that the P_N approximations (P_1 and P_3) yield somewhat more accurate predictions than the M_1 maximum entropy closure. It can also be observed that the M_1 model produces a nonphysical discontinuity in the radiative energy. Previous analysis [14] have shown that this jump is due to the inability of this first-order closure to handle radiative flux occurring in regions where bidirectional radiative transfer is important. In fact, the closure conditions for M_1 are derived under the assumption that the intensity is symmetric about the direction of the flux. Such an assumption

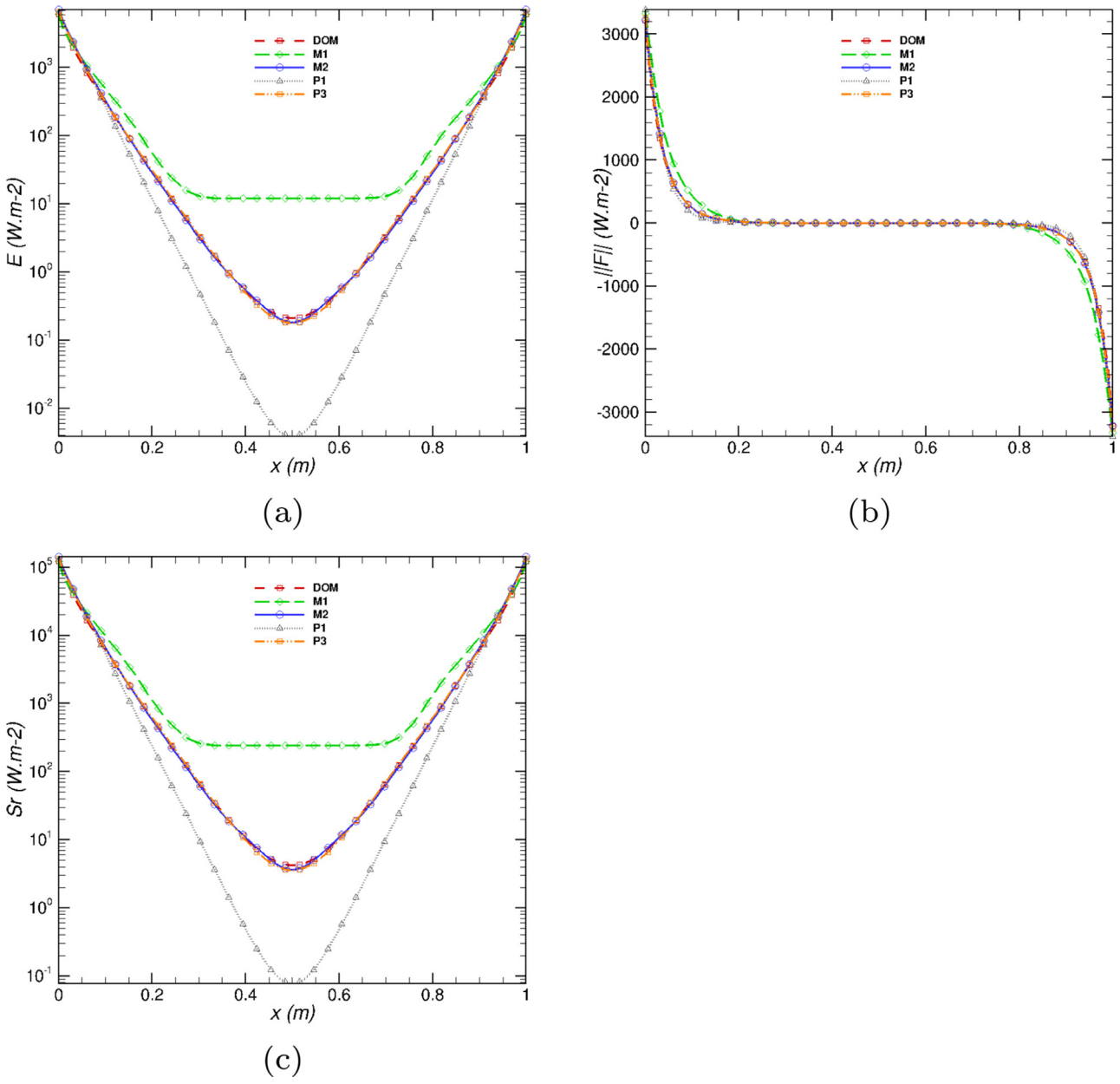

Fig. 8. Radiative transfer within square enclosure containing cold (non-emitting) and absorbing medium with wall temperatures of $T = 500$K showing numerical predictions of (a) the radiative energy, E; (b) magnitude of the radiative flux, $||F||$, (right top panel); and (c) the source of radiative energy transfer, S_r, along the centre line ($y = 0$) of the square enclosure obtained using the M_2 interpolative-based closure using a (160 × 160)-node mesh compared to the predictions of the M_1 maximum-entropy closure, P_1 and P_3 spherical harmonic closures and DOM.

is however violated in this parallel-plate test case. Nevertheless, for the larger plate separations as shown in Fig. 5, the discontinuity in the M_1 solution is less important and the predictions of the M_1 closure are closer to the exact solution than the P_1 approximation. More importantly, for both plate separation distances, the proposed second-order interpolative-based M_2 closure overcomes the inability of the M_1 model to adequately represent radiative transport in more than one direction and is significantly more accurate. The proposed closure produces a solution that is qualitatively in very good agreement with the exact solution, of similar accuracy to that of the P_1 closure for the small plate separation, and virtually identical to the P_3 model results for the larger plate separation distance.

7.1.3. Cold medium with scattering

The next one-dimensional test problem that was considered evaluated the impact of scattering on the proposed M_2 closure solutions. In this case, the previous one-dimensional problem was reconsidered with a cold medium with an absorption coefficient $\kappa = 2.0\text{m}^{-1}$ for which there is also isotropic scattering with $\sigma_s = 2.0\text{m}^{-1}$. Again, a 320-node computational mesh was used to discretize the one-dimensional domain for all computations.

The predictions for the radiative energy density, radiative heat flux, and radiative source term obtained using the proposed M_2 interpolative-based closure as well as the M_1, P_1 and P_3 moment closures and DOM with T_4 quadrature for the scattering case are compared in Fig. 6 and confirmation of the convergence of the M_2 closure on the one-dimensional meshes considered is depicted in Fig. 6(d). As an exact solution does not exist for this case, the numerical solution obtained by the DOM can be taken to approximate the exact solution. The results shown in the Fig. 6 indicate that, while the M_1 model now no longer contains a nonphysical jump in the solution for this scattering case, the predictions of the pro-

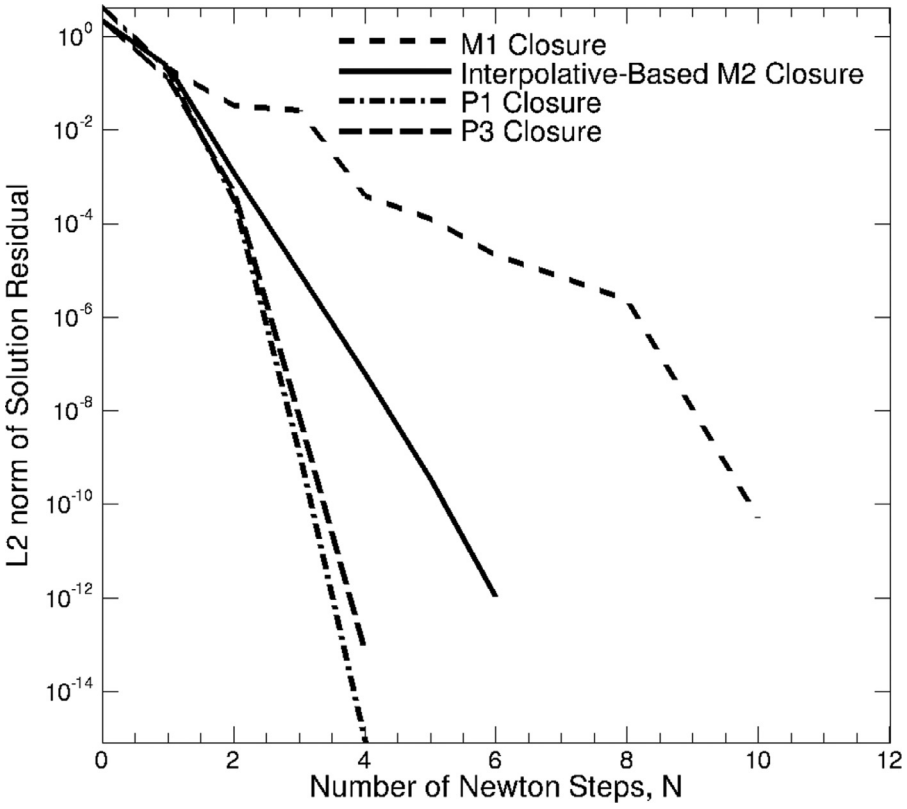

Fig. 9. Convergence of the proposed NKS iterative solution method and finite-volume scheme for the problem of radiative transfer within square enclosure containing cold (non-emitting) and absorbing medium with wall temperatures of $T = 500$K showing the L_2-norm of the normalized solution residual as a function of the number of Newton steps for the M_2 interpolative-based closure using a (160 × 160)-node mesh compared to the corresponding L_2-norm of the solution residuals for the M_1 maximum-entropy closure as well as P_1 and P_3 spherical harmonic closures.

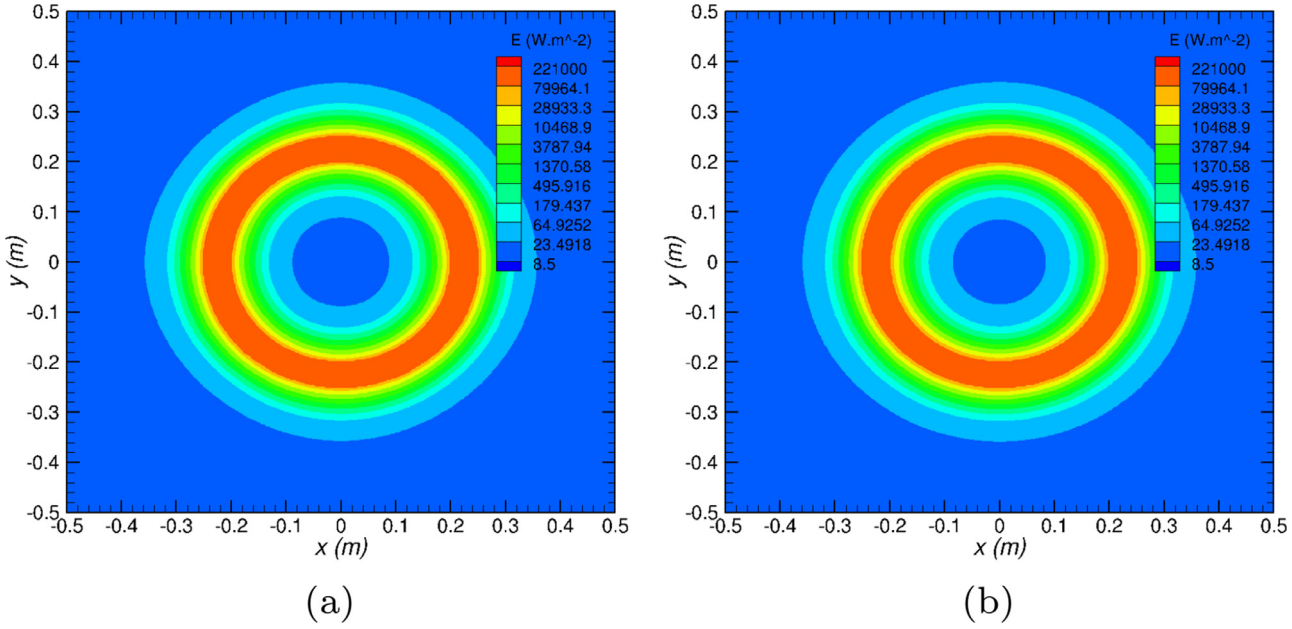

Fig. 10. Radiative transfer for a hot line source contained within a cold non-scattering background medium showing numerical predictions of the distributions of the radiative energy density as obtained using (a) the DOM and (b) the interpolative-based M_2 moment closure, on a (320 × 320)-node mesh.

posed intepolative-based M_2 closure are significantly better than those of both the M_1 and P_1 closures and lie very close to those of both the P_3 closure and "exact" solution as represented by the DOM results.

7.2. Square enclosure

The first two-dimensional test case considers a square enclosure with a cold (non-emitting) and absorbing medium. The absorption coefficient was taken to be $\kappa = 20\text{m}^{-1}$. All of the walls are taken to have identical temperatures of $T = 500$K.

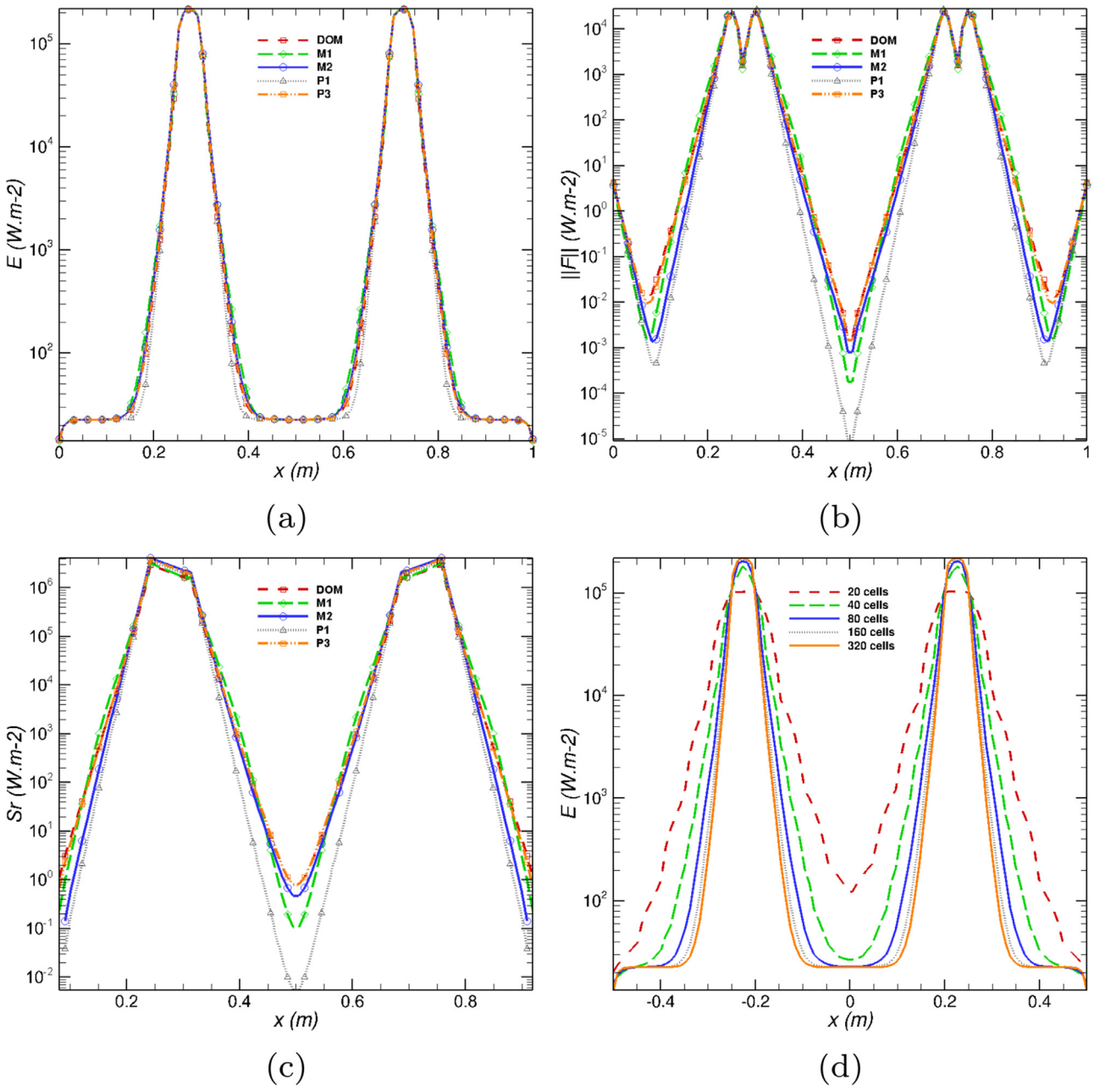

Fig. 11. Radiative transfer for a hot line source contained within a cold non-scattering background medium showing numerical predictions of (a) the radiative energy, E; (b) magnitude of the radiative flux, $||F||$; and (c) the source of radiative energy transfer, S_r, along the centre line ($y = 0$) of the square enclosure obtained using the M_2 interpolative-based closure using a (160 × 160)-node mesh compared to the predictions of the M_1 maximum-entropy closure, P_1 and P_3 spherical harmonic closures and DOM; as well as (d) the convergence of the M_2 interpolative-based closure predictions of the radiative energy for varying mesh sizes.

The predicted distributions of radiative energy density and magnitude of the radiative energy flux within the two-dimensional enclosure as obtained using the DOM and interpolative-based M_2 moment closure, respectively, are given in Fig. 7 for a (320 × 320)-node mesh. Additionally, the predictions of the proposed interpolative-based M_2 closure on the (160 × 160)-node mesh are compared to those of the M_1, P_1 and P_3 moment closures, as well as DOM in Fig. 8, where results for the radiative energy density, magnitude of the radiative flux, and radiative heat source along the centre line of the rectangular enclosure ($y = 0$) are all given. It is readily apparent from the results shown in the two sets of figures that the predictions of the newly proposed M_2 interpolative-based closure are superior to those of both the M_1 and P_1 closures and virtually equivalent to those of the P_3 model and DOM. Furthermore, there is some indication of the ray effects in the DOM T_4 results of Figs. 7(a) and this these effects are absent in the corresponding M_2 closure results.

The convergence of the proposed NKS iterative solution method and finite-volume scheme is also demonstrated for this two-dimensional problem. Fig. 9 shows the L_2-norm of the normalized solution residual as a function of the number of Newton steps for the M_2 interpolative-based closure obtained using the (160 × 160)-node mesh compared to the corresponding L_2-norm of the solution residuals for the M_1 maximum-entropy closure as well as the P_1 and P_3 spherical harmonic closures. It is quite evident that the NKS algorithm provides rapid and robust convergence to the desired solution of this problem for all of the moment closures, reducing the solution residual by more than 10 orders of magnitude in less than 10 Newton steps in all cases.

7.3. Line source problem

The last assessment of the predictive capabilities of the newly-developed approximation of the gray M_2 closure considers a two-dimensional line source problem, which consists of a cold, non-scattering medium with an absorption coefficient $\kappa = 100m^{-1}$ m^{-1}, confined within a square computational domain. At the centre of the domain, there exists a hot line source at a temperature of $T = 1,000$ K with inner radius 0.2 m and outer radius 0.25 m. Predictions of the distribution of the radiative energy density within the enclosure, obtained using the DOM with T_4 quadrature and the M_2 interpolative-based closure are compared in Fig. 10 for a (320 × 320)-node mesh. Additionally, Fig. 11 compares the predictions of the radiative energy, the magnitude of the radiative flux, and the radiative energy source term along the $y = 0$ centre line obtained using the proposed second-oder M_2 interpolative-based closure to those of the M_1, P_1, and P_3 closures, as well as the DOM with T_4 quadrature for a (160 × 160)-node computational mesh. Grid convergence for this two-dimensional case is confirmed by the results of a grid convergence study shown in Fig. 11(d) for grids ranging in size from (20 × 20) to (320 × 320) nodes. It is evident from the results shown in the two figures that both the M_2 and P_3 closures provide increased accuracy compared to their respective lower-order counterparts, i.e., the M_1 and P_1 models, respectively. Moreover, as for the square enclosure problem, the predictions of proposed M_2 interpolative-based closure are nearly identical to those of both the P_3 spherical harmonic closure and the DOM, while involving considerably fewer unknowns or degrees of freedom than either of the other two methods.

8. Conclusions

Inspired by the many desirable properties of maximum entropy closures, a new, computationally-efficient, interpolative-based, M_2 moment closure has been proposed and developed for describing radiative transport phenomena in gray media. Moment realizability and hyperbolicity of the moment equations for the proposed M_2 closure were both assessed. Unlike the interpolative-based M_2 closure proposed previously by Pichard *et al.* [19], by construction the present closure is valid for all physically realizable moments sets up to second order and also appears to be globally hyperbolic. The latter was shown numerically but not proven. Additionally, the ability of the proposed M_2 closure to predict radiative heat transfer in gray participating media for various one- and two-dimensional canonical problems has been assessed by comparing predicted solutions to those of other approximate techniques, including the M_1, P_1, and P_3 moment closures, as well as the DOM. The solutions of the newly-proposed interpolative-based M_2 closure were observed to be largely superior to those of either lower-order moment closures (i.e., the M_1 and P_1 models) and, at the very least, of equivalent accuracy to the P_3 closure, while involving considerably fewer angular moments (i.e., dependent variables). The proposed M_2 closure would seem rather promising and further investigation of the interpolative closure would therefore seem warranted. Future research will involve the extension of the interpolative-based M_2 closure to three-dimensional problems as well as the development of a non-gray (spectrally dependent) M_2 closure, which will then be validated for problems involving real-gas radiative transfer as encountered in reactive flows.

Declaration of Competing Interest

The authors have no competing interests to declare related to manuscript submission.

CRediT authorship contribution statement

Joachim A.R. Sarr: Conceptualization, Methodology, Software, Validation, Formal analysis, Investigation, Writing - original draft, Writing - review & editing. **Clinton P.T. Groth:** Resources, Supervision, Writing - original draft, Writing - review & editing.

Acknowledgements

This research was funded by grants and contracts from the Green Aviation Research and Development Network (GARDN), Southern Ontario Smart Computing for Innovation Platform (SOSCIP), as well as Pratt & Whitney Canada. The first author also received support in the form of a scholarship from the Natural Sciences and Engineering Research Council (NSERC) of Canada. Additionally, the computational resources for performing the numerical simulations reported herein were provided by the SOSCIP program as well as the SciNet High Performance Computing Consortium at the University of Toronto and Compute/Calcul Canada (the latter are funded by the Canada Foundation for Innovation (CFI) and Province of Ontario, Canada). Finally, the authors would like to thank the two reviewers for their constructive criticisms and useful suggestions for improving the clarity and quality of the revisions.

Appendix A. Necessary and sufficient conditions for realizability

Let us denote by $R^{diag}_{M_2}$ the rotation matrix which transforms the coordinates system such that the second-order tensor $N^{(2)} - N^{(1)}(N^{(1)})^T$ is diagonal. The necessary realizability conditions for the moments in the new coordinate frame, with realizability domain $\mathcal{R}^2_T$, can then be derived from those for the moments in the original frame, characterized by the realizability domain $\mathcal{R}^2$, by means of the transformation matrix, $R^{diag}_{M_2}$, as follows

$$\begin{aligned}\mathcal{R}^2_T = \{&(I'^{(0)}, I'^{(1)}, I'^{(2)}) \in \mathbb{R}^3 \times \mathbb{R}^{3\times 3}, \quad \text{s.t.} \quad I'^{(0)} \geq 0, \quad \|N'^{(1)}\| \leq 1, \\ &N'^{(2)} - N'^{(1)}(N'^{(1)})^T \geq 0, \quad (R^{diag}_{M_2}\vec{n})^T N'^{(2)} (R^{diag}_{M_2})\vec{n} \leq 1 \quad \forall \quad \|\vec{n}\| \leq 1, \\ &tr(N'^{(2)}) = 1 \quad \text{and} \quad N'^{(2)}_{ij} = N'^{(2)}_{ji}\}.\end{aligned}$$

The transformation from one set of moments to the other is illustrated in Eq. (31). Since $(N'^{(2)}_{ij} - N'^{(1)}_i N'^{(1)}_j)$ is diagonal, one can write

$$N'^{(2)}_{ij} - N'^{(1)}_i N'^{(1)}_j = \lambda_i \delta_{ij}$$

where λ_i correspond to the eigenvalues of $(N'^{(2)}_{ij} - N'^{(1)}_i N'^{(1)}_j)$, with the associated eigenvector, $\vec{\eta}_i$, coinciding with the unit vector along the coordinate axes with all entries equal to 0 except for the i^{th} entry which is equal to 1. Using the trace identity for the second-order moment, we can write

$$tr(N'^{(2)}_{ij} - N'^{(1)}_i N'^{(1)}_j) = \sum_{i=1}^{3} \lambda_i$$

$$tr(N'^{(2)}_{ij}) - tr(N'^{(1)}_i N'^{(1)}_j) = \sum_{i=1}^{3} \lambda_i$$

$$\sum_{i=1}^{3} \lambda_i = 1 - \|N^{(1)}\|^2$$

The latter identity can be further normalized by introducing normalized parameters γ_i such that

$$\lambda_i = (1 - \|N^{(1)}\|^2)\gamma_i$$

and hence

$$\sum_{i=1}^{3} \gamma_i = 1. \tag{A.1}$$

Furthermore, since $\vec{\eta}_i$ is an eigenvector of $(N'^{(2)}_{ij} - N'^{(1)}_i N'^{(1)}_j)$ with eigenvalue $\lambda_i = (1 - \|N'^{(1)}\|^2)\gamma_i$, it follows that

$$(N'^{(2)} - N'^{(1)}(N'^{(1)})^T)\vec{\eta}_i = \lambda_i \vec{\eta}_i$$
$$\vec{\eta}_i^T(N'^{(2)} - N'^{(1)}(N'^{(1)})^T)\vec{\eta}_i = \vec{\eta}_i^T \lambda_i \vec{\eta}_i$$
$$\vec{\eta}_i^T(N'^{(2)} - N'^{(1)}(N'^{(1)})^T)\vec{\eta}_i = \lambda_i \vec{\eta}_i^T \vec{\eta}_i$$
$$\vec{\eta}_i^T(N'^{(2)} - N'^{(1)}(N'^{(1)})^T)\vec{\eta}_i = \lambda_i \|\vec{\eta}_i\|$$

Since $\vec{\eta}_i$ is a unit vector, we have $\|\vec{\eta}_i\| = 1$, and,

$$\vec{\eta}_i^T(N'^{(2)} - N'^{(1)}(N'^{(1)})^T)\vec{\eta}_i = \lambda_i$$
$$\vec{\eta}_i^T(N'^{(2)} - N'^{(1)}(N'^{(1)})^T)\vec{\eta}_i = (1 - \|N'^{(1)}\|^2)\gamma_i$$

From the realizability conditions described above, we have

$$\vec{\eta}_i^T(N'^{(2)} - N'^{(1)}(N'^{(1)})^T)\vec{\eta}_i \geq 0 \quad \text{and} \quad \|N'^{(1)}\| \leq 1$$

It therefore follows that

$$\gamma_i \geq 0, \quad i = 1, \ldots, 3. \tag{A.2}$$

Appendix B. Form of the closure relation on the boundaries of the realizability domain

On the boundaries of the realizability domain for moments up to second-order, $\mathcal{R}^2_T$, in multiple space dimensions, which we denote $\partial\mathcal{R}^2_T$, the inequality constraints on the normalized first- and second-order moments become sharp, and some or all of the higher-order moments are uniquely determined in terms of the lower-order moments. More specifically $\partial\mathcal{R}^2_T$ can be written in the form

$$\begin{aligned}\partial\mathcal{R}^2_T = \{&(I'^{(0)}, I'^{(1)}, I'^{(2)}) \in \mathbb{R}^3 \times \mathbb{R}^{3\times 3}, \quad \text{s.t.} \quad I'^{(0)} \geq 0,\\ &tr(N'^{(2)}) = 1, \qquad N'^{(2)}_{ij} = N'^{(2)}_{ji} \quad \text{and} \quad \|N'^{(1)}\| = 1\\ &\text{or} \quad (R^{diag}_{M_2}\vec{n})^T(N'^{(2)} - N'^{(1)}(N'^{(1)})^T)(R^{diag}_{M_2}\vec{n}) = 0 \quad \forall \quad \vec{n} \in \mathbb{R}^3\backslash\mathbf{0}\\ &\text{or} \quad (R^{diag}_{M_2}\vec{n})^T N'^{(2)}(R^{diag}_{M_2}\vec{n}) = 1 \quad \forall \quad \|\vec{n}\| \leq 1\}.\end{aligned} \tag{B.1}$$

We will now discuss the characteristics of each of the boundaries and also present the form of the distribution in terms of the known finite set of moments up to second-order.

In the case where $\|N'^{(1)}\| = 1$, which corresponds to the so-called free-streaming limit, we have

$$\|N'^{(1)}\|^2 = (N'^{(1)})^T N'^{(1)} = 1$$
$$(N'^{(1)})^T \frac{\|I'^{(1)}\|}{I'^{(0)}} = 1$$
$$(N'^{(1)})^T I'^{(1)} = I'^{(0)}$$
$$(N'^{(1)})^T \int_{4\pi} \vec{s} I d\Omega = \int_{4\pi} (N'^{(1)})^T \vec{s} I d\Omega = \int_{4\pi} I d\Omega$$
$$\int_{4\pi} (1 - (N'^{(1)})^T \vec{s}) I d\Omega = 0.$$

Since the radiative intensity distribution is non-negative, i.e, $I \geq 0$, and by definition $1 - (N'^{(1)})^T\vec{s} \geq 0$, it therefore follows that the latter equality holds if and only if the intensity distribution I is equal to 0 everywhere except on the line $\vec{s} = N'^{(1)}$, in which case the distribution takes the form

$$I = I^{(0)}\delta(\vec{s} - N'^{(1)}). \tag{B.2}$$

The form of the distribution in Eq. (B.2) can be integrated directly to obtain analytical expression for $N'^{(3)}$

$$N'^{(3)}_{ijk} = N'^{(1)}_i N'^{(1)}_j N'^{(1)}_k. \tag{B.3}$$

Let us now consider the case where $(R^{diag}_{M_2}\vec{n})^T(N'^{(2)} - N'^{(1)}(N'^{(1)})^T)(R^{diag}_{M_2}\vec{n}) = 0 \quad \forall \quad \vec{n} \in \mathbb{R}^3\backslash\mathbf{0}$, and, in particular, the case where $R^{diag}_{M_2}\vec{n} = \vec{\eta}_i$, we then have

$$\vec{\eta}_i^T(N'^{(2)} - N'^{(1)}(N'^{(1)})^T)\vec{\eta}_i = (1 - \|N'^{(1)}\|^2)\gamma_i = 0.$$

For such relationship to hold for all $\|N'^{(1)}\| \leq 1$, we must have

$$\gamma_i = 0,$$

which corresponds to one of the edges of the triangle $(P_1P_2P_3)$ illustrated in Fig. 1; more specifically the edge (P_jP_k), $i \neq j \neq k$. Along such an edge, we can write

$$N'^{(2)}_{ii} - N'^{(1)}_i N'^{(1)}_i = 0 \tag{B.4}$$

$$I'^{(2)}_{ii} - N'^{(1)}_i I'^{(1)}_i = I'^{(2)}_{ii} - 2N'^{(1)}_i I'^{(1)}_i + \frac{(I'^{(1)}_i)^2}{I'^{(0)}} = 0 \tag{B.5}$$

$$\int_{4\pi} s_i^2 I d\Omega - 2N'^{(1)}_i \int_{4\pi} s_i I d\Omega + \left(\frac{I'^{(1)}_i}{I'^{(0)}}\right)^2 \int_{4\pi} I d\Omega = 0 \tag{B.6}$$

$$\int_{4\pi} (s_i^2 - 2N'^{(1)}_i s_i + (N'^{(1)}_i)^2) I d\Omega = 0 \tag{B.7}$$

$$\int_{4\pi} (\Omega_i - N'^{(1)}_i)^2 I d\Omega = 0. \tag{B.8}$$

Since $I \geq 0$ and by definition $(\Omega_i - N'^{(1)}_i)^2 \geq 0$, we can then conclude that the latter equality holds if and only if the intensity distribution I is equal to 0 everywhere except on the plane characterized by $s_i = N'^{(1)}_i$. In the context of moment reconstruction using the principle of maximization of entropy, the distribution then takes the form

$$I = \frac{\delta(s_i - N'^{(1)}_i)}{\exp(\boldsymbol{\alpha}^T m(\vec{s})) - 1} \tag{B.9}$$

where the monomial basis for the angular moments, $m(\vec{s})$, reads as follows

- for $i = 1$

  $m(\vec{s}) = \left[1, \Omega_2, \Omega_3, \Omega_2^2, \Omega_2\Omega_3\right]$;
- for $i = 2$

  $m(\vec{s}) = \left[1, \Omega_1, \Omega_3, \Omega_1^2, \Omega_1\Omega_3\right]$;
- for $i = 3$

  $m(\vec{s}) = \left[1, \Omega_1, \Omega_2, \Omega_1^2, \Omega_1\Omega_2\right]$.

In the case where one of γ_i, $i = 1, \ldots, 3$, is equal to one as is the case at the vertices of the triangle (P_1 P_2 P_3), then $\gamma_j = 0$, $j \in \{1, 2, 3\}$ and $j \neq i$, and from the findings in Eq. (B.4), combined with the fact that $\vec{s}$ is a unit vector, it follows that the distribution is equal to zero everywhere except on the line

$$\vec{s} = \begin{cases} (\pm\sqrt{1 - \|N'^{(1)}\|^2 + (N'^{(1)}_1)^2}, N'^{(1)}_2, N'^{(1)}_3) & \text{if} \quad \gamma_1 = 1,\\ (N'^{(1)}_1, \pm\sqrt{1 - \|N'^{(1)}\|^2 + (N'^{(1)}_2)^2}, N'^{(1)}_3) & \text{if} \quad \gamma_2 = 1,\\ (N'^{(1)}_1, N'^{(1)}_2, \pm\sqrt{1 - \|N'^{(1)}\|^2 + (N'^{(1)}_3)^2}) & \text{if} \quad \gamma_3 = 1, \end{cases} \tag{B.10}$$

and the distribution is then uniquely determined by a Dirac delta or a combination of Dirac deltas of the form

$$I_{P_i} = I'^{(0)}\left[\rho_i^+\delta(\Omega_i - x_i^+) + \rho_i^-\delta(\Omega_i - x_i^-)\right]\delta(\Omega_j - N'^{(1)}_j)\delta(\Omega_k - N'^{(1)}_k), \tag{B.11}$$

where $(i, j, k) \in (1,2,3)$ with $i \neq j \neq k$ and ρ_i^+, ρ_i^-, x_i^+ and x_i^- are some parameters which must be determined from the realizablity constraints for moments up to first-order (since the second-order moments depend on the lower-order moments in this case), and read as follows

$$x_i^{\pm} = \pm\sqrt{1 - \|N'^{(1)}\|^2 + (N_i'^{(1)})^2}, \quad \text{and} \quad \rho_i^{\pm} = \frac{N_i'^{(1)} - x_i^{\mp}}{2x_i^{\pm}}. \tag{B.12}$$

Appendix C. Sufficiency of realizability conditions for moments up to second-order

Let us consider a point P lying within the triangle $(P_1P_2P_3)$ (see Fig. 1) with corresponding set of moments $(I'^{(0)}, I'^{(1)}.I'^{(2)})$, an reconstruct the distribution at the vertices of the triangle, given in Eq. (B.11), such that they exactly reproduce the zeroth and first-order moments, $I'^{(0)}$ and $I'^{(1)}$, respectively. We may then write the distribution at the point P as a convex combination of the distributions at the vertices of the triangle using the barycentric coordinates, γ_i, of the latter, as

$$I_P = \sum_{i=1}^{3} \gamma_i I_{P_i}, \tag{C.1}$$

From the above defined form of the distribution, it is clear, using Eq. (A.1), that I_P reproduces $I'^{(0)}$ and $I'^{(1)}$, since I_{P_i}, $i = 1, \ldots, 3$ reproduce such moments. For the second-order moment, $I'^{(2)}$, we have

$$\int_{4\pi} \vec{s}^2 I_P \mathrm{d}\Omega = \sum_{i=1}^{3} \gamma_i \int_{4\pi} \vec{s}^2 I_{P_i} \mathrm{d}\Omega.$$

Computing the second-order moments at the vertices yields

$$\int_{4\pi} \Omega_m \Omega_n I_{P_i} \mathrm{d}\Omega = I'^{(0)} \int_{4\pi} \Omega_m \Omega_n \big[\rho_i^+ \delta(\Omega_i - x_i^+) + \rho_i^- \delta(\Omega_i - x_i^-)\big] \delta(\Omega_j - N_j'^{(1)}) \delta(\Omega_k - N_k'^{(1)}) d\Omega$$

$$\int_{4\pi} \Omega_m \Omega_n I_{P_i} \mathrm{d}\Omega = I'^{(0)} \begin{cases} \rho_i^+ \left(x_i^+\right)^2 + \rho_i^- \left(x_i^-\right)^2 & \text{if} \quad m = n = i, \\ \left(N_m'^{(1)}\right)^2 & \text{if} \quad m = n \neq i, \\ N_m'^{(1)} N_n'^{(1)} & \text{if} \quad m \neq n, \end{cases}$$

For simplicity, we set $I'^{(0)} = 1$ in the remainder of the derivation. We will now distinguish two cases:

- Case 1: $m \neq n$

$$\int_{4\pi} \Omega_m \Omega_n I_P \mathrm{d}\Omega = \sum_{i=1}^{3} \gamma_i N_m'^{(1)} N_n'^{(1)},$$

$$\int_{4\pi} \Omega_m \Omega_n I_P \mathrm{d}\Omega = N_m'^{(1)} N_n'^{(1)} \sum_{i=1}^{3} \gamma_i.$$

Using Eq. (A.1), we then obtain

$$\int_{4\pi} \Omega_m \Omega_n I_P d\Omega = N_m'^{(1)} N_n'^{(1)}. \tag{C.2}$$

- Case 2: $m = n = i$

$$\int_{4\pi} (\Omega_m)^2 I_P \mathrm{d}\Omega = \gamma_i \left[\rho_m^+ \left(x_m^+\right)^2 + \rho_m^- \left(x_m^-\right)^2\right] + \gamma_j \left(N_m'^{(1)}\right)^2 + \gamma_k \left(N_m'^{(1)}\right)^2,$$

$$\int_{4\pi} (\Omega_m)^2 I_P \mathrm{d}\Omega = \gamma_i \left[(\rho_m^+ + \rho_m^-)\left(x_m^+\right)^2\right] + \gamma_j \left(N_m'^{(1)}\right)^2 + \gamma_k \left(N_m'^{(1)}\right)^2.$$

From Eq. (B.12), it is clear that $\rho_m^+ + \rho_m^- = 1$, and therefore Using Eq. (A.1), we then obtain

$$\int_{4\pi} (\Omega_m)^2 I_P \mathrm{d}\Omega = \gamma_i \left(x_m^+\right)^2 + \gamma_j \left(N_m'^{(1)}\right)^2 + \gamma_k \left(N_m'^{(1)}\right)^2,$$

$$\int_{4\pi} (\Omega_m)^2 I_P \mathrm{d}\Omega = \gamma_i \left(1 - \|N'^{(1)}\|^2 + (N_m'^{(1)})^2\right) + \gamma_j \left(N_m'^{(1)}\right)^2 + \gamma_k \left(N_m'^{(1)}\right)^2,$$

$$\int_{4\pi} (\Omega_m)^2 I_P \mathrm{d}\Omega = (\gamma_i + \gamma_j + \gamma_k) \left(N_m'^{(1)}\right)^2 + \gamma_i \left(1 - \|N'^{(1)}\|^2\right).$$

Again using Eq. (A.1), we then obtain

$$\int_{4\pi} (\Omega_m)^2 I_P \mathrm{d}\Omega = \left(N_m'^{(1)}\right)^2 + \gamma_i \left(1 - \|N'^{(1)}\|^2\right) \tag{C.3}$$

From the results given in Eq. (C.2) and (C.3), it is clear that I_P (with $P \in \mathcal{R}_T^2$), given in Eq. (C.1) also reproduces $I'^{(2)}$.

Appendix D. Procedure for computing derivatives of the angular moments with respect to other angular moments

In our proposed interpolations, direct computation of the interpolating functions from the pre-computed solutions of the optimization problem for entropy maximization yields undetermined expressions in the isotropic limit as well as on the boundaries of the realizable domain. Applying l'Hopital's rule is such cases results in an expression in terms of the derivatives of the highest-order moments with respect to the lower-order moments, which can be expressed as follows

$$\frac{\partial I^{(3)}}{\partial I^{(j)}} = \sum_{i=0}^{9} \frac{\partial I^{(3)}}{\partial \alpha_i} \frac{\partial \alpha_i}{\partial I^{(j)}}, \quad j = 0, \ldots, 2, \tag{D.1}$$

where we have used the chain rule for derivatives.

The derivatives of the Lagrange multipliers with respect to the lower-order moments can be obtained by exploiting the following relationships

$$\begin{aligned} \frac{\partial I^{(0)}}{\partial I^{(0)}} &= \sum_{i=0}^{9} \frac{\partial I^{(0)}}{\partial \alpha_i} \frac{\partial \alpha_i}{\partial I^{(0)}} = 1, \\ \frac{\partial I^{(0)}}{\partial I_j^{(1)}} &= \sum_{i=0}^{9} \frac{\partial I^{(0)}}{\partial \alpha_i} \frac{\partial \alpha_i}{\partial I_j^{(1)}} = 0, \\ \frac{\partial I^{(0)}}{\partial I_{jk}^{(2)}} &= \sum_{i=0}^{9} \frac{\partial I^{(0)}}{\partial \alpha_i} \frac{\partial \alpha_i}{\partial I_{jk}^{(2)}} = 0, \end{aligned} \tag{D.2}$$

$$\begin{aligned} \frac{\partial I_j^{(1)}}{\partial I^{(0)}} &= \sum_{i=0}^{9} \frac{\partial I_j^{(1)}}{\partial \alpha_i} \frac{\partial \alpha_i}{\partial I^{(0)}} = 0, \\ \frac{\partial I_j^{(1)}}{\partial I_k^{(1)}} &= \sum_{i=0}^{9} \frac{\partial I^{(1)}}{\partial \alpha_i} \frac{\partial \alpha_i}{\partial I^{(1)}} = \delta_{jk}, \\ \frac{\partial I_j^{(1)}}{\partial I_{kl}^{(2)}} &= \sum_{i=0}^{9} \frac{\partial I_j^{(1)}}{\partial \alpha_i} \frac{\partial \alpha_i}{\partial I_{kl}^{(2)}} = 0, \end{aligned} \tag{D.3}$$

$$\begin{aligned} \frac{\partial I_{jk}^{(2)}}{\partial I^{(0)}} &= \sum_{i=0}^{9} \frac{\partial I_{jk}^{(2)}}{\partial \alpha_i} \frac{\partial \alpha_i}{\partial I^{(0)}} = 0, \\ \frac{\partial I_{jk}^{(2)}}{\partial I_l^{(1)}} &= \sum_{i=0}^{9} \frac{\partial I_{jk}^{(2)}}{\partial \alpha_i} \frac{\partial \alpha_i}{\partial I_l^{(1)}} = 0, \\ \frac{\partial I_{jk}^{(2)}}{\partial I_{lm}^{(2)}} &= \sum_{i=0}^{9} \frac{\partial I_{jk}^{(2)}}{\partial \alpha_i} \frac{\partial \alpha_i}{\partial I_{lm}^{(2)}} = \delta_{jl}\delta_{km}. \end{aligned} \tag{D.4}$$

The above relationships can be rewritten in matrix form as follows

$$HA = I \tag{D.5}$$

where

$$H = \begin{bmatrix} \frac{\partial I^{(0)}}{\partial \alpha_1} & \frac{\partial I^{(0)}}{\partial \alpha_2} & \cdots & \frac{\partial I^{(0)}}{\partial \alpha_9} \\ \frac{\partial I_1^{(1)}}{\partial \alpha_1} & \frac{\partial I_1^{(1)}}{\partial \alpha_2} & \cdots & \frac{\partial I_1^{(1)}}{\partial \alpha_9} \\ \vdots & \vdots & \cdots & \vdots \\ \frac{\partial I_3^{(1)}}{\partial \alpha_1} & \frac{\partial I_3^{(1)}}{\partial \alpha_2} & \cdots & \frac{\partial I_3^{(1)}}{\partial \alpha_9} \\ \frac{\partial I_{11}^{(2)}}{\partial \alpha_1} & \frac{\partial I_{11}^{(2)}}{\partial \alpha_2} & \cdots & \frac{\partial I_{11}^{(2)}}{\partial \alpha_9} \\ \vdots & \vdots & \cdots & \vdots \\ \frac{\partial I_{23}^{(2)}}{\partial \alpha_1} & \frac{\partial I_{23}^{(2)}}{\partial \alpha_2} & \cdots & \frac{\partial I_{23}^{(2)}}{\partial \alpha_9} \end{bmatrix} \tag{D.6}$$

and

$$A = \begin{bmatrix} \frac{\partial \alpha_1}{\partial I^{(0)}} & \frac{\partial \alpha_1}{\partial I_1^{(1)}} & \cdots & \frac{\partial \alpha_1}{\partial I_3^{(1)}} & \frac{\partial \alpha_1}{\partial I_{11}^{(2)}} & \cdots & \frac{\partial \alpha_1}{\partial I_{23}^{(2)}} \\ \frac{\partial \alpha_2}{\partial I^{(0)}} & \frac{\partial \alpha_2}{\partial I_1^{(1)}} & \cdots & \frac{\partial \alpha_2}{\partial I_3^{(1)}} & \frac{\partial \alpha_2}{\partial I_{11}^{(2)}} & \cdots & \frac{\partial \alpha_2}{\partial I_{23}^{(2)}} \\ \vdots & \vdots & \cdots & \vdots & \vdots & \vdots & \vdots \\ \frac{\partial \alpha_4}{\partial I^{(0)}} & \frac{\partial \alpha_4}{\partial I_1^{(1)}} & \cdots & \frac{\partial \alpha_4}{\partial I_3^{(1)}} & \frac{\partial \alpha_4}{\partial I_{11}^{(2)}} & \cdots & \frac{\partial \alpha_4}{\partial I_{23}^{(2)}} \\ \frac{\partial \alpha_5}{\partial I^{(0)}} & \frac{\partial \alpha_5}{\partial I_1^{(1)}} & \cdots & \frac{\partial \alpha_5}{\partial I_3^{(1)}} & \frac{\partial \alpha_5}{\partial I_{11}^{(2)}} & \cdots & \frac{\partial \alpha_5}{\partial I_{23}^{(2)}} \\ \vdots & \vdots & \cdots & \vdots & \vdots & \vdots & \vdots \\ \frac{\partial \alpha_9}{\partial I^{(0)}} & \frac{\partial \alpha_9}{\partial I_1^{(1)}} & \cdots & \frac{\partial \alpha_9}{\partial I_3^{(1)}} & \frac{\partial \alpha_9}{\partial I_{11}^{(2)}} & \cdots & \frac{\partial \alpha_9}{\partial I_{23}^{(2)}} \end{bmatrix} \tag{D.7}$$

and I is a 9×9 identity matrix. The matrix A can then be written as

$$A = H^{-1}. \tag{D.8}$$

References

[1] Modest MF. Radiative heat transfer. 2nd. New York: Academic Press; 2003.
[2] W A Fiveland WA. Discrete-ordinates solutions of the radiative transport equation for rectangular enclosures. J Heat Transfer 1984;106(4):699–706.
[3] Charest MRJ, Groth CPT, Gülder ÖL. Solution of the equation of radiative transfer using a newton-krylov approach and adaptive mesh refinement. J Comput Phys 2012;231:3023–40.
[4] Grad H. On the kinetic theory of rarefied gases. Commun Pure Appl Math 1949;2:331–407.
[5] Jeans JH. The equations of radiative transfer of energy. Mon Not R Astron Soc 1917;78(1):28–36.
[6] Mazumder S, Modest MF. A probability density function approach to modeling turbulence-radiation interactions in nonluminous flames. Int J Heat Mass Transf 1999;42(6):971–91.
[7] Li G, Modest MF. Importance of turbulence-radiation interactions in turbulent diffusion jet flames. J Heat Transfer 2003;125(5):831–8.
[8] Modest MF, Mehta RS. Modeling absorption TRI in optically thick eddies. Proceedings of Eurotherm78 - Computational Thermal Radiation in Participating Media II 2006;78:225–34.
[9] Gupta A, Modest MF, Haworth DC. Large-eddy simulation of turbulence-radiation interactions in a turbulent planar channel flow. J Heat Transfer 2009;131(6):061704–1–061704–8.
[10] Menguc MP, Viskanta R. Radiative transfer in three-dimensional rectangular enclosures containing inhomogeneous anisotropically scattering media. J Quant Spectrosc Radiat Transfer 1985;33:533–49.
[11] Fletcher JK. The solution of the multigroup neutron transport equation using spherical harmonics. Nucl Sci Eng 1983;84(1):33–46.
[12] Dubroca B, Feugeas J-L. Theoretical and numerical study on a moment closure hierarchy for the radiative transfer equation. SIAM J Numer Anal 1999;329:915–20.
[13] Jaynes ET. Information theory and statistical mechanics. Physical Review 1957;106:620–30.
[14] Brunner TA, Holloway JP. One-dimensional Riemann solvers and the maximum entropy closure. J Quant Spectrosc Radiat Transfer 2001;69:543–66.
[15] Tencer J, Howell J. A parametric study of the accuracy of several radiative transfer solution methods for a set of 2-D benchmark problems. In: Proceedings of the ASME 2013 summer heat transfer conference, Minneapolis; 2013.
[16] Hauck CD. High-order entropy-based closures for linear transport in slab geometry. Report. Oak Ridge National Laboratory; 2010.
[17] Hauck CD. High-order entropy-based closures for linear transport in slab geometry. Commun Math Sci 2011;9(1):187–205.
[18] Monreal P, Frank M. Higher order minimum entropy approximations in radiative transfer. arXiv Online Article. Cornell University Library; 2008.
[19] Pichard T, Alldredge GW, Brull S, Dubroca B, Frank M. An approximation of the M_2 closure: application to radiotherapy dose simulation. J Sci Comput 2017;71(1):71–108.
[20] McDonald JG, Groth CPT. Towards realizable hyperbolic moment closures for viscous heat-conducting gas flows based on a maximum-entropy distribution. Continuum Mech Thermodyn 2013;25:573–603.
[21] McDonald JG, Torrilhon M. Affordable robust moment closures for CFD based on the maximum-entropy hierarchy. J Comput Phys 2013;251:500–23.
[22] Kershaw D. Flux limiting nature's own way. Technical Report. Lawrence Livermore Laboratory; 1976.
[23] Lathrop KD, Carlson BG. Discrete ordinates angular quadrature of the neutron transport equation. Report LA. Los Alamos Scientific Laboratory; 1965.
[24] Thurgood CP, Pollard A, Becker HA. The T_N quadrature set for the discrete ordinates method. ASME Journal of Heat Transfer 1995;117(4):1068–70.
[25] Coelho PJ. The role of ray effects and false scattering on the accuracy of the standard and modified discrete ordinates methods. J Quant Spectrosc Radiat Transfer 2002;73(2–5):231–8.
[26] Coelho PJ. Bounded skew high-order resolution schemes for the discrete ordinates method. J Comput Phys 2002;175(2):412–37.
[27] Sakami M, El Kasmi A, Charette A. Analysis of radiative heat transfer in complex two-dimensional enclosures with obstacles using the modified discrete ordinates method. J Heat Transfer 2001;123(5):892–900.
[28] Koch R, Krebs W, Wittig S, Viskanta R. Discrete ordinates quadrature schemes for multidimensional radiative transfer. J Quant Spectrosc Radiat Transfer 1995;53(4):353–72.
[29] Ramankutty MA, Crosbie AL. Modified discrete ordinates solution of radiative transfer in two-dimensional rectangular enclosures. J Quant Spectrosc Radiat Transfer 1997;57(1):107–40.
[30] Amiri H, Mansouri SH, Coelho PJ. Application of the modified discrete ordinates method with the concept of blocked-off region to irregular geometries. Int J Therm Sci 2011;50(4):515–24.
[31] Groth CPT, McDonald JG. Towards physically-realizable and hyperbolic moment closures for kinetic theory. Continuum Mech Thermodyn 2009;21(6):467–93.
[32] Marshak RE. Note on the spherical harmonic method as applied to the milne problem for a sphere. Physical Review 1947;71(7):443–6.
[33] Arpaci VS, Gözüm D. Thermal stability of radiating fluids: the Bénard problem. Physics of Fluids 1973;16(5):581–8.
[34] Levermore C. Relating eddington factors to flux limiters. J Quant Spectrosc Radiat Transfer 1984;31(2):149–60.
[35] Li R, Li W. 3D B_2 model for radiative transfer equation part I: modelling. Int J Numer Anal Model 2020;17(1):118–50.
[36] Monreal P. Moment realizability and Kershaw closures in radiative transfer. RWTH Aachen University; 2012.
[37] Johnson S.G. The NLopt nonlinear-optimization package. http://github.com/stevengj/nlopt; 2014.
[38] Kraft D. A software package for sequential quadratic programming. Technical Report. Institut fõr Dynamik der Flugsysteme, Oberpfaffenhofen; 1988.
[39] Kraft D. Algorithm 733; tomp—Fortran modules for optimal control calculations. ACM Trans Math Software 1994;20(3):262–81.
[40] Alldredge GW, Hauck CD, O'Leary DP, Tits AL. Adaptive change of basis in entropy-based moment closures for linear kinetic equations. J Comput Phys 2014;258:489–508.
[41] Alldredge GW, Hauck CD, Tits AL. High-order entropy-based closures for linear transport in slab geometry II: a computational study of the optimization problem. SIAM Journal on Scientific Computing 2012;34(4):B361–91.
[42] Abramov RV. An improved algorithm for the multidimensional moment-constrained maximum entropy problem. J Comput Phys 2007;226:621–44.
[43] Abramov RV. The multidimensional moment-constrained maximum entropy problem: a BFGS algorithm with constraint scaling. J Comput Phys 2009;228:96–108.
[44] Liu F, Swithenbank J, Garbett ES. The boundary condition of the P_N approximation used to solve the radiative transfer equation. Int J Heat Mass Transf 1992;35(8):2043–52.
[45] Lax PD. Hyperbolic systems of conservation laws and the mathematical theory of shock waves. CMBS–NSF Regional Conference Series in Applied Mathematics, 11. Philadelphia: SIAM; 1973.
[46] Levermore CD. Moment closure hierarchies for kinetic theories. J Stat Phys 1996;83:1021–65.
[47] Godunov SK. Finite-difference method for numerical computations of discontinuous solutions of the equations of fluid dynamics. Matematicheskii Sbornik 1959;47:271–306.
[48] Sachdev JS, Groth CPT, Gottlieb JJ. A parallel solution-adaptive scheme for predicting multi-phase core flows in solid propellant rocket motors. Int J Comut Fluid Dyn 2005;19(2):159–77.
[49] Gao X, Groth CPT. A parallel adaptive mesh refinement algorithm for predicting turbulent non-premixed combusting flows. Int J Comut Fluid Dyn 2006;20(5):349–57.
[50] Gao X, Northrup SA, Groth CPT. Parallel solution-adaptive method for two-dimensional non-premixed combusting flows. Progress in Computational Fluid Dynamics 2011;11(2):76–95.
[51] McDonald JG, Sachdev JS, Groth CPT. Application of Gaussian moment closure to micro-scale flows with moving and embedded boundaries. AIAA Journal 2014;51(9):1839–57.

[52] Harten A. High resolution schemes for hyperbolic conservation laws. J Comput Phys 1983;49:357–93.
[53] Einfeldt B. On Godunov-type methods for gas dynamics. SIAM J Numer Anal 1988;25:294–318.
[54] Barth TJ. Recent developments in high order k-exact reconstruction on unstructured meshes. Paper. AIAA; 1993.
[55] Venkatakrishnan V. On the accuracy of limiters and convergence to steady state solutions. Paper. AIAA; 1993.
[56] Zhang ZJ, Groth CPT. Parallel high-order anisotropic block-based adaptive mesh refinement finite-volume scheme. Paper. AIAA; 2011.
[57] Williamschen MJ, Groth CPT. Parallel anisotropic block-based adaptive mesh refinement algorithm for three-dimensional flows. Paper. AIAA; 2013.
[58] Hryniewicki MK, Groth CPT, Gottlieb JJ. Parallel implicit anisotropic block--based adaptive mesh refinement finite-volume scheme for the study of fully resolved oblique shock wave reflections. Shock Waves 2015;25(4):371–86.
[59] Freret L, Groth CPT. Anisotropic non-uniform block-based adaptive mesh refinement for three-dimensional inviscid and viscous flows. Paper. AIAA; 2015.
[60] Freret L, Ivan L, De Sterck H, Groth CPT. High-order finite-volume method with block-based AMR for magnetohydrodynamics flows. J Sci Comput 2019;79(1):176–208.
[61] Freret L, Williamsche M, Groth C.P.T. Parallel anisotropic non-uniform block-based adaptive mesh refinement for three-dimensional inviscid and viscous flows. submitted to the Journal of Computational Physics; 2020.
[62] Gao X, Groth CPT. A parallel solution-adaptive method for three-dimensional turbulent non-premixed combusting flows. J Comput Phys 2010;229(5):3250–75.
[63] Groth CPT, Northrup SA. Parallel implicit adaptive mesh refinement scheme for body-fitted multi-block mesh. Paper. AIAA; 2005.
[64] Charest MRJ, Groth CPT, Gülder ÖL. A computational framework for predicting laminar reactive flows with soot formation. Combust Theor Model 2010;14(6):793–825.
[65] Saad Y, Schultz MH. GMRES: a generalized minimal residual algorithm for solving nonsymmetric linear equations. SIAM Journal for Scientific and Statistical Computing 1986;7(3):856–69.
[66] Saad Y. Krylov subspace methods on supercomputers. SIAM Journal for Scientific and Statistical Computing 1989;10(6):1200–32.
[67] Brown PN, Saad Y. Hybrid Krylov methods for nonlinear systems of equations. SIAM Journal for Scientific and Statistical Computing 1990;11(3):450–81.
[68] Saad Y. Iterative methods for sparse linear systems. Boston: PWS Publishing Company; 1996.
[69] Mulder WA, van Leer B. Experiments with implicit upwind methods for the euler equations. J Comput Phys 1985;59:232–46.